

Deuterium fractionation and the degree of ionization in the R Coronae Australis molecular cloud core

I.M. Anderson¹, P. Caselli², L.K. Haikala^{1,3}, and J. Harju¹

¹ Observatory, P.O. Box 14, FIN-00014 University of Helsinki, Finland

² Osservatorio Astrofisico di Arcetri, Largo E. Fermi 5, I-50125 Firenze, Italy

³ Swedish-ESO Submillimetre Telescope, European Southern Observatory, Casilla 19001, Santiago, Chile

Received 24 November 1998 / Accepted 4 January 1999

Abstract. The fractionation of D and ¹³C in HCO⁺ was investigated in the R Coronae Australis molecular cloud core. The distributions of H¹³CO⁺ and DCO⁺ were found to be morphologically similar but their column density maxima were found to lie in different locations.

The H¹³CO⁺/HC¹⁸O⁺ abundance ratio was found to vary little from 10 within the mapped region, in excellent agreement with the ¹³CO/C¹⁸O abundance ratios derived earlier towards the cloud by Harjunpää & Mattila (1996). This corroborates the close relationship between HCO⁺ and CO predicted by the chemistry models.

The DCO⁺/HCO⁺ abundance ratio ranges from 0.006 to 0.04, being lowest towards two locations near the embedded infrared source IRS 7 where the kinetic temperature, as derived from methyl acetylene (CH₃CCH) observations, is somewhat elevated. The variation of the degree of deuterium fractionation within the core is due to an increase in the kinetic temperature near the cluster of newly born stars. This temperature rise results in two effects: Firstly, the reaction H₂D⁺ → H₃⁺ becomes faster; and secondly, an intensified desorption from grain surfaces increases the abundance of neutral atoms and molecules in the gas phase leading to the destruction of H₃⁺ and H₂D⁺ ions. Both processes decrease the DCO⁺/HCO⁺ abundance ratio. Far from the active region the derived abundances of neutral species indicate the presence of depletion onto grain surfaces.

The observations suggest furthermore that the fractional electron abundance, $\chi(e^-)$, is lowest in the dense clump near IRS 7. This region also exhibits a low degree of gas phase depletion. In fact, increased fractional abundances of neutral species such as atomic oxygen and CO lead to a decrease in the [H₃⁺]/[HCO⁺] abundance ratio which is directly proportional to $\chi(e^-)$.

Key words: molecular processes – ISM: abundances – ISM: clouds – ISM: molecules – ISM: individual objects: R CrA core

1. Introduction

Deuterium enhancement in HCO⁺ and other molecules is expected to occur in the coldest regions of molecular clouds (Watson 1977). Consequently DCO⁺ maps have been used for identifying dense cores at an early stage of evolution when heating from newly born stars is not significant (e.g. Loren et al. 1990).

Besides being dependent on the temperature, the DCO⁺/HCO⁺ abundance ratio also depends on the abundances of electrons and neutral species destroying their chemical precursors H₃⁺ and H₂D⁺. Due to this dependence the DCO⁺/HCO⁺ ratio has been frequently used for estimates of the electron abundance (e.g. Guélin et al. 1977, 1982; Watson et al. 1978; Wootten et al. 1982; Dalgarno & Lepp 1984). The cosmic ray ionization rate has usually been estimated from the [HCO⁺]/[CO] abundance ratio (e.g. Wootten et al. 1979). In recent studies these estimates have been improved by implementing newly determined electron recombination rates for H₃⁺ and H₂D⁺ (Sundström et al. 1994; Larsson et al. 1996) and comprehensive chemistry models (Caselli et al. 1998, hereafter CWTH; Williams et al. 1998; Bergin et al. 1999). Both the fractional electron abundance and the cosmic ray ionization rate are important parameters in cloud dynamics: The former determines the time scale of ambipolar diffusion and the latter is the major heating source of the molecular gas (see e.g. CWTH and references therein).

There have been few studies where the spatial distribution of the deuterium fractionation has been investigated within a cloud (Guélin et al. 1982; Wootten et al. 1982, Bergin et al. 1998). Such studies are, however, essential in disentangling the effects of various processes, such as local heating and increased turbulence due to star formation, on fractionation. It should be noted that the cosmic ray ionization rate is likely to be constant over length scales typical of molecular clouds (Strong 1987; Bertsch et al. 1993).

In the present work we have investigated the variation of the DCO⁺/HCO⁺ abundance ratio in the R Coronae Australis (hereafter R CrA) cloud core, a nearby site of low to intermediate mass star formation which contains several dense clumps (Wilking et al. 1997; Harju et al. 1993, hereafter H93; Anderson et al. 1997a, hereafter A97a; Anderson et al. 1997b, here-

after A97b). The effect of kinetic temperature on the degree of DCO⁺ fractionation within the core was investigated and the results were compared with the predictions of chemistry models. By employing a simplified chemistry model we have been able to estimate the fractional abundances of electrons and neutral agents taking part in the destruction of the H₃⁺ and H₂D⁺ ions at several locations.

The plan of this paper is as follows: in Sect. 2 we describe the observations and in Sect. 3 we present the observational results. In Sect. 4 we discuss the ¹³C and D fractionation ratios for HCO⁺ and give estimates for the fractional electron abundance. In Sect. 5 the results are discussed and in Sect. 6 the conclusions are summarized. In Appendix A we list the principal reactions involved in the DCO⁺ - HCO⁺ chemistry and derive the formulae used in the analysis of Sect. 4. Finally, in Appendix B we describe the method used in the determination of the rotational temperature of methyl acetylene.

2. Observations

The observations were made over the period February - May 1996 and in June 1997 with the SEST¹ on La Silla in Chile. The cloud was mapped over 982 positions with a spacing of 15'' simultaneously in the H¹³CO⁺($J = 1 - 0$) and DCO⁺($J = 2 - 1$) transitions at 3 and 2 mm respectively in the frequency switching mode with a frequency throw of 8 MHz. The spacing was chosen so that the DCO⁺($J = 2 - 1$) map is fully sampled. During the observations the typical system temperatures of the 3 and 2 mm receivers were 130 and 150 K, respectively. Both SIS receivers were connected to a 2000 channel acousto-optical spectrometer which was split in two bands of 43 MHz each. The map was centred on the embedded infrared source IRS 7 ($\alpha_{1950.0} = 18^h58^m33.0^s$, $\delta_{1950.0} = -37^\circ01'43''$). This is by far the most comprehensive and detailed DCO⁺ - HCO⁺ map done to date.

The HC¹⁸O⁺($J = 1 - 0$) and DCO⁺($J = 3 - 2$) lines were observed simultaneously with 3 and 1.3 mm SIS receivers, respectively, towards 12 positions in the frequency switching mode. The typical system temperature at $\lambda = 1.4$ mm was 220 K. The CH₃CCH($J_K = 5_K - 4_K$) and ($J_K = 8_K - 7_K$) ladders at 3 and 2 mm, respectively, were observed towards selected positions in the position switching mode. The OFF-position, with coordinates $\alpha_{1950.0} = 18^h57^m40.0^s$, $\delta_{1950.0} = -37^\circ05'00''$, was chosen in the void near S CrA.

Calibration was achieved by the chopper wheel method. The pointing and focus were checked at 3-4 hour intervals in the SiO($v = 1$, $J = 2 - 1$) maser line towards AH Sco and VX Sgr. The pointing accuracy was typically found to be 3''.

A summary of the observed lines, frequencies, antenna half-power beam widths (BW), main beam efficiencies (η_M) and the velocity resolutions (Δv_{AOS}) corresponding to the channel separations of the spectrometers used is given in Table 1. Further details of the equipment can be found in Booth et al. (1989) and in the SEST manual (<http://www.ls.eso.org/lasilla/Telescopes/SEST>).

Table 1. The frequencies, half power beam widths, main beam efficiencies and spectrometer channel separation (in velocity units) for the observed transitions.

Transition	Frequency (MHz)	BW (")	η_M	Δv_{AOS} (km/s)
H ¹³ CO ⁺ (1 - 0)	86754.330	57	0.75	0.145
DCO ⁺ (2 - 1)	144077.319	35	0.66	0.087
HC ¹⁸ O ⁺ (1 - 0)	85162.157	57	0.75	0.147
DCO ⁺ (3 - 2)	216112.605	25	0.61	0.058
CH ₃ CCH(5 ₁ - 4 ₁)	85455.622	57	0.75	0.147
CH ₃ CCH(8 ₁ - 7 ₁)	136725.397	37	0.67	0.092

3. Results

3.1. H¹³CO⁺($J = 1 - 0$) and DCO⁺($J = 2 - 1$) observations

The distributions of the H¹³CO⁺($J = 1 - 0$) and DCO⁺($J = 2 - 1$) line emission towards the R CrA core are presented in Figs. 1 and 2. These figures show three channel maps between 4, 5, 6 and 7 km s⁻¹ and the integrated intensity (T_A^*) maps in the velocity range 4 to 7.5 km s⁻¹, superposed on the C¹⁸O($J = 1 - 0$) emission map detailed in H93. Indicated in these figures are the locations of some prominent young stars and Herbig-Haro objects. Although the H¹³CO⁺ and DCO⁺ maps are morphologically similar, the integrated intensity maxima lie in different locations. The dense core near IRS 7 ('A2' in H93) is markedly more intense in the H¹³CO⁺ emission than in the DCO⁺ emission. However, the northwestern clump south of TY CrA ('A1' in H93) and especially the southeastern condensation (near the tip of 'SW jaw' in H93) are evidently regions of strong DCO⁺ emission. There is a DCO⁺ and H¹³CO⁺ emission void of some 1.5' \times 1.5' centered on (45'', -130''), the feature being more evident in DCO⁺. This void is near but not coincident with the 'central hole' detected in C¹⁸O($J = 1 - 0$) (H93).

Since both transitions are probably optically thin, their integrated intensity ratio is proportional to the DCO⁺/H¹³CO⁺ column density ratio, provided that the excitation temperatures, T_{ex} , for the two isotopomers are the same. For example, the proportionality factor ranges from 1.2 to 0.7 when T_{ex} rises from 5 to 10 K. Figs. 1 and 2 thus suggest that the column density ratio DCO⁺/H¹³CO⁺ varies over the mapped region. To confirm this, estimates of the excitation temperature are required.

3.2. DCO⁺($J = 3 - 2$) and HC¹⁸O⁺($J = 1 - 0$) observations

In order to determine excitation temperatures, 12 positions with different DCO⁺($J = 2 - 1$)/H¹³CO⁺($J = 1 - 0$) intensity ratios were observed in DCO⁺($J = 3 - 2$). These positions were observed simultaneously in HC¹⁸O($J = 1 - 0$) to verify that the H¹³CO⁺($J = 1 - 0$) emission was optically thin and, in addition, to search for any indication of ¹³C fractionation. The latter eventuality would complicate the determination of

¹ SEST=Swedish-ESO Submillimetre Telescope

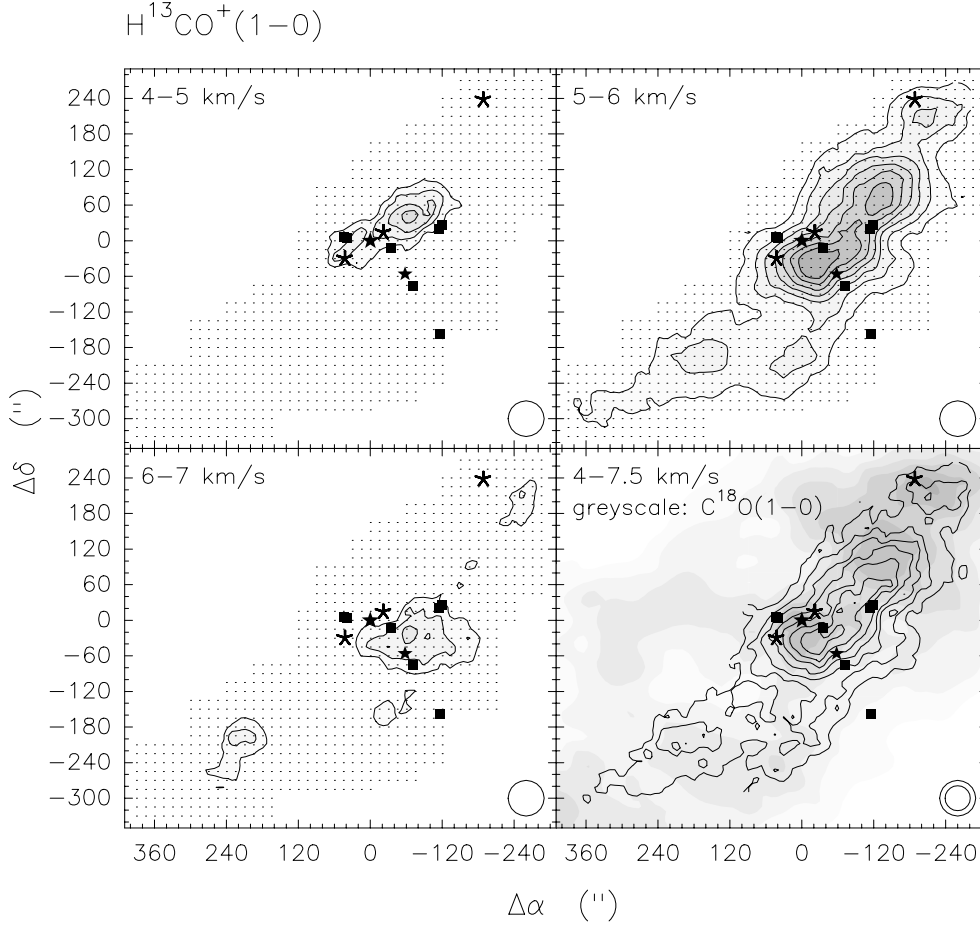


Fig. 1. H¹³CO⁺ ($J = 1 - 0$) channel maps and a superposition of the H¹³CO⁺ ($J = 1 - 0$) (contour) and C¹⁸O ($J = 1 - 0$) (greyscale) integrated intensity maps over the velocity range 4.0 - 7.5 km/s. The C¹⁸O data are from H93. The coordinate offsets are relative to the embedded infrared source IRS 7 ($\alpha_{1950.0} = 18^h 58^m 33.0^s$, $\delta_{1950.0} = -37^\circ 01' 43''$). The locations of IRS 7 and the infrared source HH100-IR are denoted by stars, the T Tauri star T CrA (left) and the Herbig Ae/Be stars R CrA (right) and TY CrA (up) are denoted by asterisks and the Herbig-Haro objects HH104A and B (east), HH104 C and D (west), HH98 (centre), HH100 (southwest) and HH97 (further southwest) are denoted by squares. The beamsizes are indicated in the bottom right of each map.

the HCO⁺ column densities from the H¹³CO⁺ data. The locations of the selected positions are indicated in the finding chart presented in Fig. 3.

The H¹³CO⁺ ($J = 1 - 0$), HC¹⁸O⁺ ($J = 1 - 0$), DCO⁺ ($J = 2 - 1$) and DCO⁺ ($J = 3 - 2$) spectra towards the 12 selected positions are shown in Fig. 4. For the two former transitions the beamsizes are similar, i.e. 57''. Since the HC¹⁸O⁺ emission is comparatively weak, these spectra have been smoothed once and multiplied by 5.5, the solar system $[^{13}\text{C}^{16}\text{O}]/[^{12}\text{C}^{18}\text{O}]$ abundance ratio. It is evident from Fig. 4 that the $[\text{H}^{13}\text{CO}^+]/[\text{HC}^{18}\text{O}^+]$ abundance ratio in R CrA exceeds the solar system value. This indicates the presence of ¹³C fractionation (see Sect. 4.1).

The excitation temperatures for DCO⁺ ($J = 2 - 1$) and ($J = 3 - 2$) were derived from their integrated intensity ratios assuming LTE and optically thin emission. The different beam-source coupling efficiencies due to different beam sizes were taken into account by assuming that the source fills the main beam of the SEST at 2mm. The same assumption was used in conversion from T_A^* to the radiation temperature T_R^* needed in the derivation of the column densities.

If the derived excitation temperatures are valid for all the observed isotopomers, then the DCO⁺, H¹³CO⁺ and HC¹⁸O⁺ column densities can be determined from their respective integrated line intensities. In order to directly compare the DCO⁺

column densities with those of H¹³CO⁺, we have convolved the DCO⁺ ($J = 2 - 1$) data set to correspond to observations made with a 57'' Gaussian beam, the HPBW for H¹³CO⁺ ($J = 1 - 0$) observations at SEST.

The results are given in Table 2, the columns of which correspond to: (1) ID number of the position as denoted in Fig. 3; (2) R.A. and Decl. offsets with respect to IRS 7 ($\alpha_{1950.0} = 18^h 58^m 33.0^s$, $\delta_{1950.0} = -37^\circ 01' 43''$); (3) excitation temperature; (4), (5) and (6) DCO⁺, H¹³CO⁺ and HC¹⁸O⁺ column densities, respectively; (7) H¹³CO⁺/HC¹⁸O⁺ column density ratio; (8) DCO⁺ column densities derived from the convolved data; (9) and (10) the column density ratios DCO⁺/H¹³CO⁺ and DCO⁺/HC¹⁸O⁺, respectively.

From Table 2 it can be seen that the calculated H¹³CO⁺/HC¹⁸O⁺ column density ratios vary little over the mapped region. With the exception of position 11 at (210'', -195'') where the HC¹⁸O⁺ line is weakest, the H¹³CO⁺/HC¹⁸O⁺ ratio lies between 6.7 and 13.6. The average ratio and its standard deviation, position 11 excluded, is 10.5 ± 2.2 .

The convolved DCO⁺/H¹³CO⁺ ratios range from 0.3 at (0'', 0'') and (-15'', -30'') (the dense core) to about 2 at (240'', -255''). The highest values, 1.4 - 2.0, are obtained in the southeastern condensation. If the very uncertain value at (210'', -195'') is omitted, the corresponding ratios between

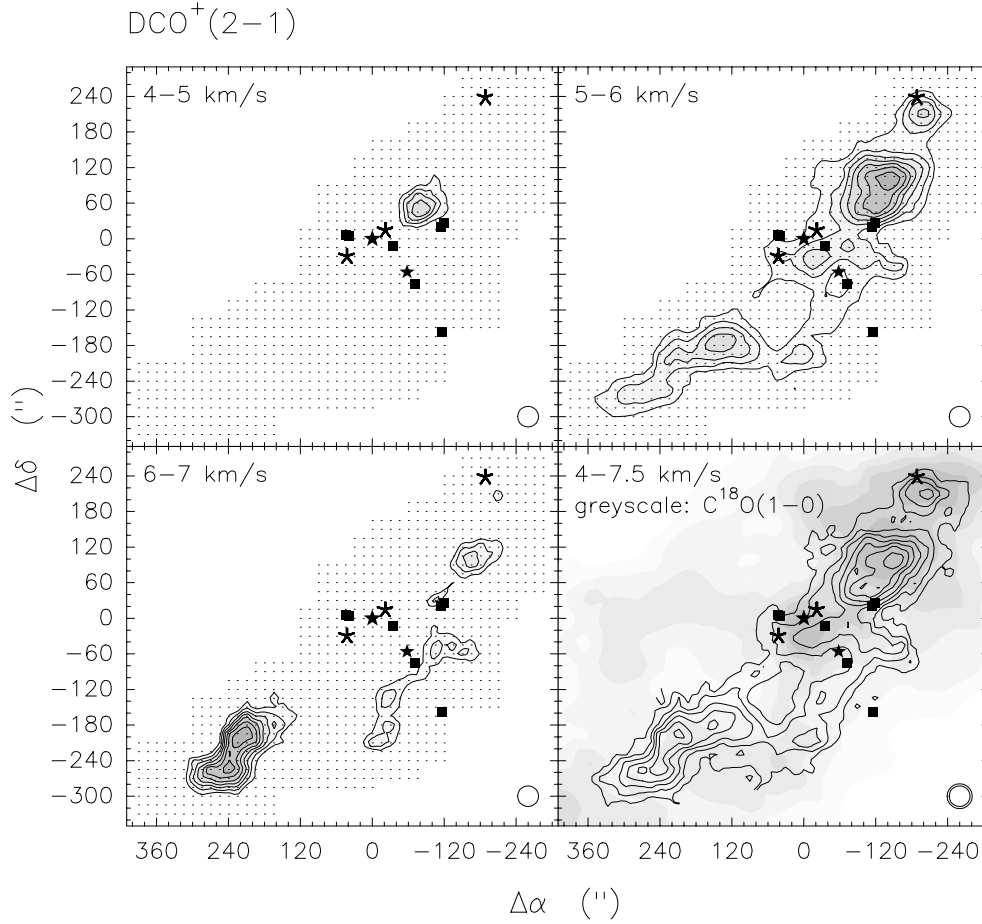


Fig. 2. Same as Fig. 1 but for DCO⁺ ($J = 2 - 1$).

Table 2. The excitation temperature, DCO⁺, H¹³CO⁺, HC¹⁸O⁺ column density, H¹³CO⁺/HC¹⁸O⁺ column density ratio, DCO⁺ column density derived from the convolved data and its ratios with the H¹³CO⁺ and HC¹⁸O⁺ column densities towards selected positions.

(1) No.	(2) $\Delta\alpha$	(3) $\Delta\delta$	(4) T_{ex}	(5) $N(\text{DCO}^+)$	(6) $N(\text{H}^{13}\text{CO}^+)$	(7) $N(\text{HC}^{18}\text{O}^+)$	(8) $\frac{[\text{H}^{13}\text{CO}^+]}{[\text{HC}^{18}\text{O}^+]}$	(9) $N(\text{DCO}^+)$ (conv.)	(10) $\frac{[\text{DCO}^+]}{[\text{H}^{13}\text{CO}^+]}$	(11) $\frac{[\text{DCO}^+]}{[\text{HC}^{18}\text{O}^+]}$
	(")	(")	(K)	$\cdot 10^{-11}$ (cm^{-2})	$\cdot 10^{-11}$ (cm^{-2})	$\cdot 10^{-11}$ (cm^{-2})		$\cdot 10^{-11}$ (cm^{-2})		
1	-210	210	6.0	14.2±0.4	12.1±0.3	1.0±0.2	12.6±2.3	11.8±0.4	0.98±0.06	12.4± 2.5
2	-150	90	7.2	19.5±0.3	19.0±0.2	1.8±0.1	10.8±0.7	18.6±0.4	0.98±0.03	10.5± 0.8
3	-105	-45	6.2	9.6±0.4	13.3±0.3	1.0±0.2	13.6±2.7	9.7±0.4	0.73±0.05	10.0± 2.2
4	-105	60	7.1	23.2±0.3	23.3±0.1	2.3±0.2	10.3±0.8	20.4±0.3	0.88±0.02	9.0± 0.8
5	-75	30	7.2	12.7±0.3	25.3±0.2	2.1±0.1	12.0±0.9	12.5±0.3	0.50±0.02	5.9± 0.6
6	-60	-15	7.3	11.1±0.3	25.8±0.2	2.5±0.1	10.4±0.7	10.1±0.3	0.39±0.01	4.1± 0.4
7	-15	-30	9.2	10.7±0.2	29.1±0.2	2.8±0.1	10.4±0.6	9.1±0.3	0.31±0.01	3.3± 0.3
8	0	-210	5.3	14.9±0.6	8.9±0.3	1.3±0.2	6.7±1.0	12.7±0.7	1.43±0.12	9.5± 1.6
9	0	0	8.7	7.6±0.2	22.7±0.2	1.8±0.2	12.4±1.1	6.8±0.3	0.30±0.01	3.7± 0.5
10	150	-180	6.1	18.5±0.4	8.7±0.3	1.1±0.2	7.8±1.8	16.3±0.5	1.87±0.11	14.6± 3.3
11	210	-195	6.6	19.3±0.4	11.4±0.2	0.5±0.2	25.2±9.5	17.2±0.4	1.51±0.06	38±15
12	240	-255	6.5	17.3±0.4	7.7±0.3	0.9±0.2	8.3±2.4	15.4±0.4	1.99±0.12	16.6± 4.6

DCO⁺ and HC¹⁸O⁺ range from 3.3 and 3.7 at (-15", -30") and (0", 0") to 16.6 at (240", -255").

3.3. CH₃CCH ($J = 5 - 4$) and ($J = 8 - 7$) observations

The $J = 5 - 4$, $K = 0, 1, 2, 3$ and $J = 8 - 7$, $K = 0, 1, 2, 3$ transitions of CH₃CCH were observed towards positions 1, 2, 4, 7, 9, 11 and 12. The lines were, however, not detected towards

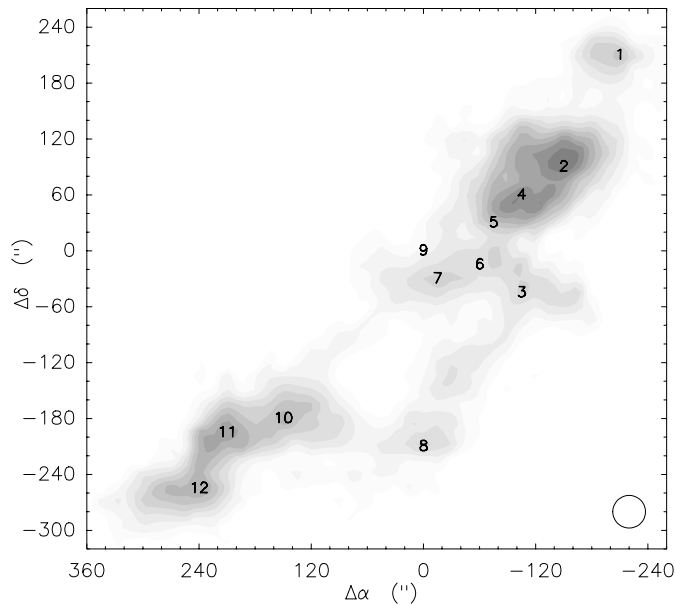


Fig. 3. The locations of the 12 positions selected for accurate column density determination superposed on the DCO⁺($J = 2 - 1$) integrated intensity map. These identification numbers are used in Figs. 4, 5, 6 and 7 and Tables 2, 3 and 4.

positions 1, 11 and 12. The RMS noise level attained in these locations were 0.015, 0.014 and 0.010 K, respectively. The $J = 5 - 4$ and $J = 8 - 7$ spectra towards the four positions where CH₃CCH was detected are shown in Figs. 5 and 6. The Gaussian fits to the $K = 0, 1, 2$ and 3 components and their residuals are indicated in the figures.

The rotational temperatures, T_{rot} , for CH₃CCH were derived from the combined $J = 5 - 4$ and $J = 8 - 7$ data using the rotational diagram method, as described in Appendix B. The rotational diagrams and the results of the least-squares fits are shown in Fig. 7. The derived values of T_{rot} and CH₃CCH column densities (N) are indicated in the top right and bottom left of each diagram, respectively. The ‘Q-value’ i.e. the value of the incomplete Gamma function, provides a quantitative measure of the significance of the fit (see Press et al. 1986). The fit is believable if $Q > 0.1$, becoming progressively more credible as Q approaches unity.

One can see in Fig. 7 that the values of T_{rot} , which closely approximate the gas kinetic temperature (e.g. Bergin et al. 1994), range from about 17 to 30 K towards the four positions where CH₃CCH was detected. The temperature in the north-western part of the R CrA core thus seems to be elevated with respect to the typical dark cloud conditions. Locations 2 and 4, with high DCO⁺/C¹⁸O and DCO⁺/HC¹⁸O⁺ column density ratios, are, however, cooler than locations 7 and 9 with low DCO⁺/C¹⁸O and DCO⁺/HC¹⁸O⁺ column density ratios.

3.4. Previous C¹⁸O($J = 1 - 0$) data

We have used the C¹⁸O($J = 1 - 0$) mapping of H93 in order to estimate the [HCO⁺]/[CO] ratios. The data set was con-

verted to correspond to a 57'' Gaussian beam, and interpolation was used to determine the C¹⁸O column densities towards the selected positions. H93 could determine the excitation temperatures from the pair C¹⁸O($J = 1 - 0$)/C¹⁷O($J = 1 - 0$) only towards a few locations in the R CrA core because the emission was found to be optically thin and no $J = 2 - 1$ lines were observed (see their Tables 2 and 3). Two of these locations lie close our selected positions. These are (−240'', 240'') (near position 1) with $T_{\text{ex}} = 13.8 \pm 3.1$ K, and (40'', −240'') (near position 8) with $T_{\text{ex}} = 14.5 \pm 5.8$ K. We therefore assume that $T_{\text{ex}} = 14$ K towards positions 1 and 8.

Since C¹⁸O is probably thermalized in dense gas, we assume that the excitation temperature towards positions 2, 4, 7 and 9 is equal to the kinetic temperature as derived from CH₃CCH. It is conceivable that the temperature is also elevated towards the intermediate positions 3, 5, and 6 near the cloud centre, and we assume there an excitation temperature of 17 K.

On account of its distance from any newly born stars, the kinetic temperature towards the southeastern clump probably approaches a value typical of dark clouds. The excitation temperatures derived by H93 towards (80'', −80'') and several locations towards the ‘tail’ further southeast range from 5.5 to 13.4 K, supporting the notion of low temperatures far from the centre of activity. We assume an excitation temperature of 13 K towards positions 10, 11 and 12. A temperature slightly higher than 10 K seems reasonable also on the basis of the DCO⁺($J = 2 - 1$)/($J = 3 - 2$) line ratios (see below).

The assumed values of T_{ex} are summarized in Column (3) of Table 3. The other columns of Table 3 are: (4) the derived C¹⁸O column density in the velocity range 4 – 7.5 km s^{−1}; (5) the fractional CO abundance, $\chi(\text{CO})$, derived using the relation between $N(\text{H}_2)$ and $N(\text{C}^{18}\text{O})$ determined in CrA by Harjunpää & Mattila (1996) assuming $N(\text{H}_2)/E(J - K) = 5.4 \cdot 10^{21}$ cm^{−2}mag^{−1}) and an average [C¹⁸O]/[C¹⁶O] ratio of 560 ± 25 as in the local ISM (Wilson & Rood 1994); (6) and (7) the column density ratios DCO⁺/C¹⁸O and HC¹⁸O⁺/C¹⁸O, respectively.

The adopted linear relation between the C¹⁸O column density and the colour excess $E(J - K)$ implies a practically constant fractional CO abundance in the R CrA core: $\chi(\text{CO}) = 7 - 8 \cdot 10^{-5}$. It should be noted, however, that the relation was originally determined up to the colour excess $E(J - K) = 5$ or visual extinction $A_V \approx 26^m$, corresponding to a C¹⁸O column density of about $3 \cdot 10^{15}$ cm^{−2}. Therefore, the derived values of $\chi(\text{CO})$ are most reliable towards the southeastern part of the core (positions 8, 10, 11 and 12), where the column densities are about $3 \cdot 10^{15}$ cm^{−2}. Towards the core centre and the north-eastern clump, the C¹⁸O column densities are higher by a factor of 2 or 3. Current gas phase chemical models where no depletion occurs (e.g. Lee et al. 1996) predict $\chi(\text{CO}) = 1.5 \cdot 10^{-4}$. However, CWTH showed that $\chi(\text{CO})$ is inversely dependent on the depletion factor f_D . Therefore, the C¹⁸O data suggest that CO is indeed depleted by a factor of about 2 towards the coldest southern core. Similar degrees of CO depletion have been recently measured by Kramer et al. (1999) in the densest and coldest part of the IC5146 molecular cloud. The possible deviations of

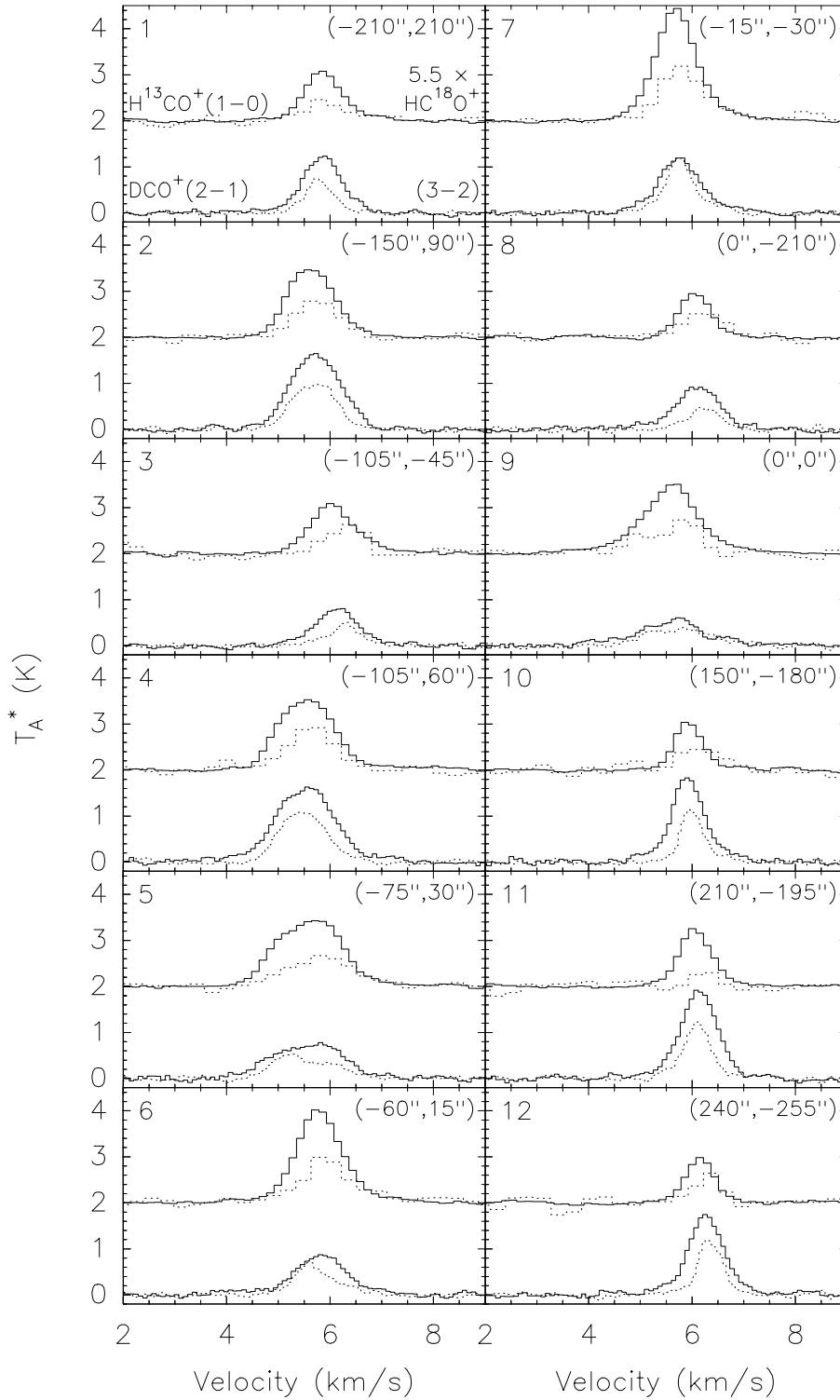


Fig. 4. H¹³CO⁺ ($J = 1 - 0$) (upper solid), $5.5 \times$ HC¹⁸O⁺ ($J = 1 - 0$) (upper dashed), DCO⁺ ($J = 2 - 1$) (lower solid) and DCO⁺ ($J = 3 - 2$) (lower dashed) spectra towards 12 positions in the R CrA core. The offsets are with respect to IRS 7, whilst the numbers in the top left of each panel correspond to the positions depicted in Fig. 3.

$\chi(\text{CO})$ from the values derived here towards the northwestern high column density regions is discussed in Sect. 5.

From Table 3 it can be seen that the column density ratio DCO⁺/C¹⁸O ranges from $0.7 \cdot 10^{-4}$ at $(0'', 0'')$ (towards IRS 7) to $5.6 \cdot 10^{-4}$ at $(150'', -180'')$. The low ratios ($2.0 \cdot 10^{-4}$ or less) are found near IRS 7 and the Coronet cluster (positions 6, 7 and 9) and in the northern clump near TY CrA and HD

176386 (position 1). The highest values ($5.2 \cdot 10^{-4}$ or higher) are found towards the southeastern condensation (positions 10, 11 and 12).

The derived HC¹⁸O⁺/C¹⁸O column density ratios also vary. However, there seems to be no clear difference between the active regions and the supposed ‘quiescent’ regions further away from the newly born stars. If position 11 is dropped, the ra-

Table 3. The assumed excitation temperatures for C¹⁸O, the derived C¹⁸O column densities, fractional CO abundances, and the column density ratios DCO⁺/C¹⁸O and HC¹⁸O⁺/C¹⁸O. The C¹⁸O and DCO⁺ data sets are convolved to correspond the 57'' beam used in the HC¹⁸O⁺ observations.

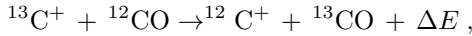
(1) No.	(2) $\Delta\alpha$	$\Delta\delta$	(3) T_{ex} (C ¹⁸ O)	(4) $N(\text{C}^{18}\text{O})$ (conv.) $\cdot 10^{-15}$ (cm ⁻²)	(5) $\chi(\text{CO})$ $\cdot 10^5$	(6) $\frac{[\text{DCO}^+]}{[\text{C}^{18}\text{O}]}$ $\cdot 10^4$	(7) $\frac{[\text{HC}^{18}\text{O}^+]}{[\text{C}^{18}\text{O}]}$ $\cdot 10^5$
	($''$)	($''$)	(K)				
1	-210	210	14	5.91±0.07	7.9±1.1	2.0±0.1	1.6±0.3
2	-150	90	18	6.65±0.11	8.0±1.1	2.8±0.1	2.7±0.2
3	-105	-45	17	4.10±0.12	7.6±1.5	2.4±0.2	2.4±0.5
4	-105	60	17	5.63±0.08	7.9±1.1	3.6±0.1	4.0±0.3
5	-75	30	17	5.12±0.07	7.8±1.2	2.5±0.1	4.1±0.4
6	-60	-15	17	5.38±0.09	7.8±1.2	1.9±0.1	4.6±0.4
7	-15	-30	24	7.91±0.09	8.2±1.0	1.2±0.1	3.5±0.2
8	0	-210	14	3.37±0.06	7.3±1.4	3.8±0.3	4.0±0.5
9	0	0	30	9.28±0.06	8.3±0.9	0.7±0.1	2.0±0.2
10	150	-180	13	2.93±0.10	7.1±1.7	5.6±0.3	3.8±0.9
11	210	-195	13	3.25±0.08	7.3±1.5	5.3±0.2	1.4±0.5
12	240	-255	13	2.98±0.10	7.1±1.6	5.2±0.3	3.1±0.9

tio ranges from $1.5 \cdot 10^{-5}$ at $(-210'', 210'')$ to $4.6 \cdot 10^{-5}$ at $(-60'', -15'')$ with an average and standard deviation of $(3.3 \pm 1.0) \cdot 10^{-5}$.

4. Chemical fractionation and electron abundances

4.1. ¹³C fractionation

The two isotopomers DCO⁺ and H¹³CO⁺ selected for this study have frequently been used in deuterium fractionation studies. The reason is that the most common isotopomer H¹²C¹⁶O⁺ is usually optically thick whilst D¹³CO⁺ is difficult to detect because of its rarity. However, this selection does lead to a complication: As HCO⁺ is produced directly from CO and the reaction



is exothermic with $\Delta E/k = 35$ K (Watson 1977), substantial ¹³C fractionation is to be expected in cold, dense gas (Watson 1977, Smith & Adams 1984). A similar exchange reaction between the ¹⁶O and ¹⁸O isotopes is inhibited under interstellar cloud conditions due to the high ionization potential of atomic oxygen. Therefore, in the interiors of dark clouds, where selective photodissociation (Bally & Langer 1982) is probably prevented, the C¹⁸O/CO and HC¹⁸O⁺/HCO⁺ abundance ratios should be equal to the interstellar [¹⁸O]/[¹⁶O] ratio.

In Sect. 3.2 the H¹³CO⁺/HC¹⁸O⁺ ratio in the R CrA core was given as 10.5 ± 2.2 . Harjunpää & Mattila (1996) determined the ¹³CO and C¹⁸O column densities towards seven highly reddened background stars in the R CrA cloud. With the exception of one location on the outskirts of the cloud, they found the mean ¹³CO/C¹⁸O abundance ratio over six positions to be 9.2 ± 1.3 . Therefore, it would appear that the ¹³C fractionation in CO is manifest in HCO⁺, as predicted by ion-molecule chemistry. Furthermore, this result shows that H¹³CO⁺ can be used reli-

ably for HCO⁺ abundance estimates only if the degree of ¹³C fractionation is known.

4.2. DCO⁺/HCO⁺ abundance ratios and the fractional electron abundances

In the following we derive the HCO⁺ column densities from H¹³CO⁺ rather than from HC¹⁸O⁺ because of the higher signal to noise ratios of the former lines. The average H¹³CO⁺/HC¹⁸O⁺ ratio given above, and the average [¹⁸O]/[¹⁶O] ratio in the local ISM (560 ± 25 , Wilson & Rood 1994) are used in the conversion of the H¹³CO⁺ column densities to those of the common isotope HCO⁺ and for the derivation of the DCO⁺/HCO⁺ column density ratios. Note that the resulting [HCO⁺]/[H¹³CO⁺] abundance ratio is 53, and thus fairly close to the value of 60 used in several previous studies (e.g. Wootten et al. 1982; Bergin et al. 1999).

The derived DCO⁺/HCO⁺ and HCO⁺/CO column density ratios and the fractional HCO⁺ abundances, $\chi(\text{HCO}^+)$ ($\equiv [\text{HCO}^+]/[\text{H}_2]$), are presented in Columns (3), (4) and (5) of Table 4, respectively. The fractional HCO⁺ abundances were estimated by using the fractional CO abundances, $\chi(\text{CO})$, derived in the previous subsection. The linewidths from Gaussian fits to the DCO⁺ ($J = 2 - 1$) lines, discussed in Sect. 5, are given in Column (6) of Table 4, and in Column (7) the rotational temperatures for CH₃CCH are presented.

The DCO⁺/HCO⁺ abundance ratio varies from 0.006 to about 0.04. The minimum value is towards $(0'', 0'')$ (IRS 7) and $(-15'', -30'')$ (the dense clump near IRS 7, A97a). The maximum is found towards the southeastern clump (positions 10, 11 and 12) further away from the cluster of newly born stars. The ratio increases systematically with angular separation from IRS 7. The results near IRS 7 are consistent with those of Wootten et al. (1982) who derived a DCO⁺/HCO⁺ ratio of 0.008

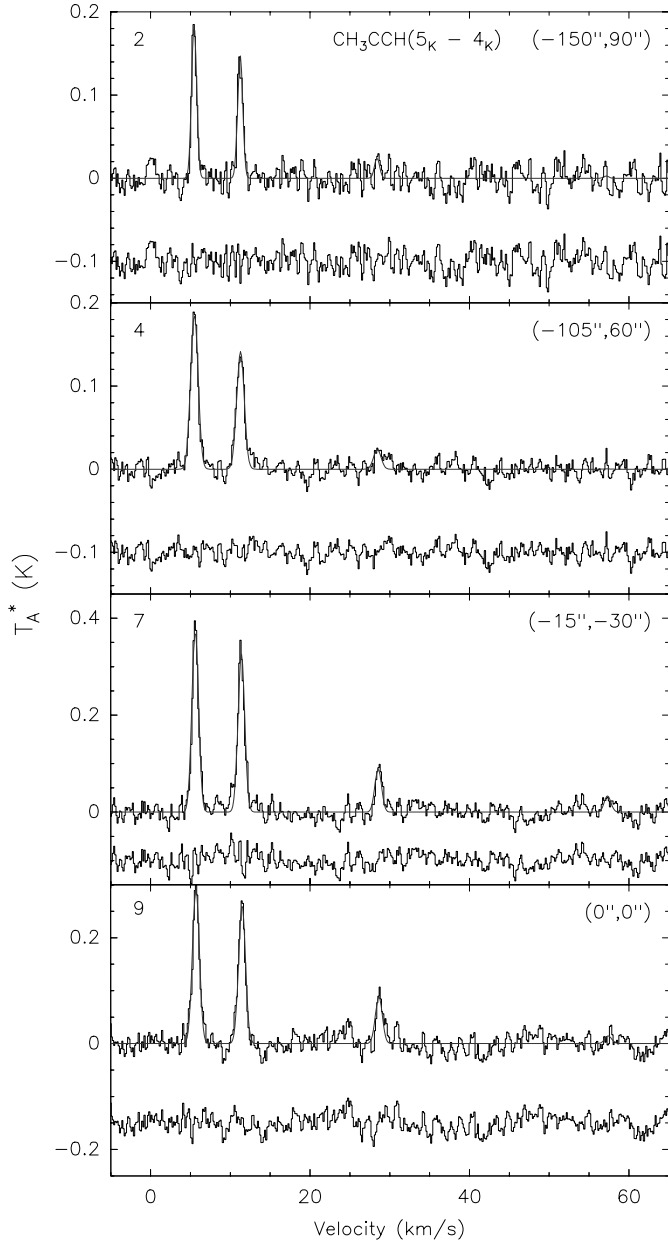


Fig. 5. CH₃CCH($J = 5 - 4$) spectra towards the positions 2, 4, 7 and 9 in the R CrA core. Gaussian fits to the spectra are indicated. The residuals of the fits are plotted below the spectra. The LSR velocity is correct only for the $K = 0$ component at the left, which was used as the frequency reference.

and a kinetic temperature of 29 K at the offset ($-7''$, $-25''$) from our map centre.

The HCO⁺/CO abundance ratio lies in the range $2.0 \cdot 10^{-5} - 4.7 \cdot 10^{-5}$. The highest values are found at locations 4, 5, 6 and 7.

The remaining parameters given in Table 4, in Columns (8)–(12), were derived using the simplified chemistry model described in Appendix A. This derivation was subject to the following constraints:

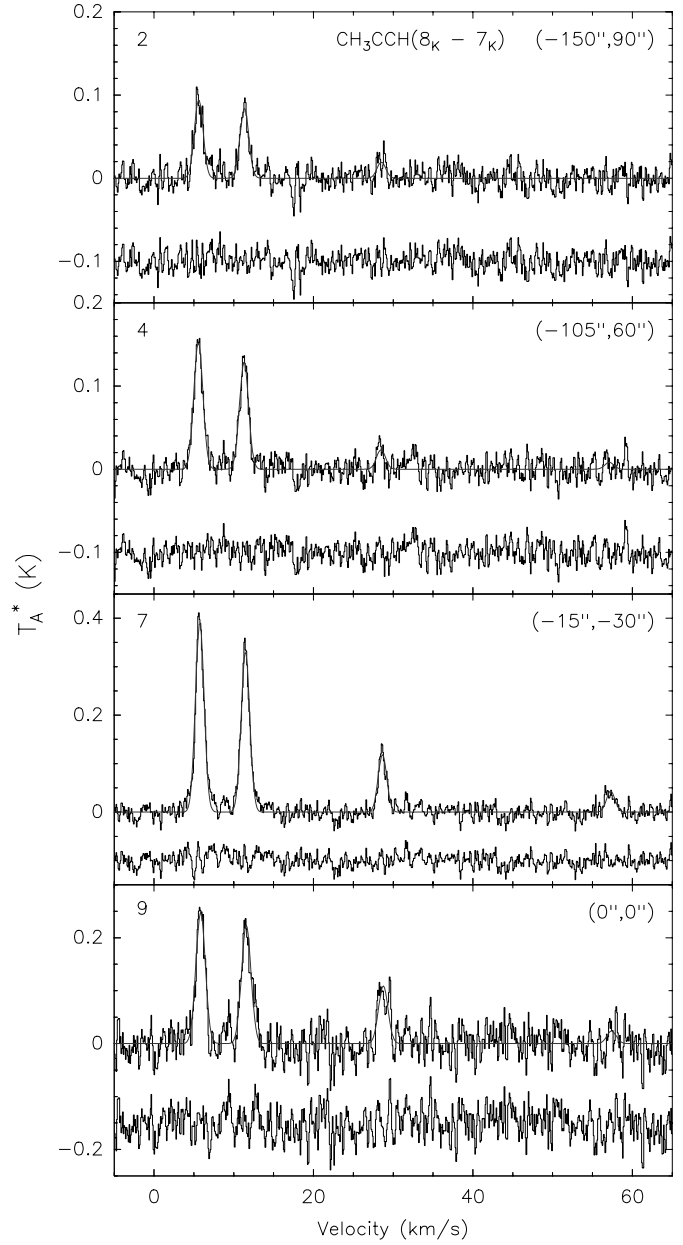


Fig. 6. Same as Fig. 5 but for CH₃CCH($J = 8 - 7$).

1) As discussed in Sect. A.1, the $[\text{H}_3^+]/[\text{HCO}^+]$ abundance ratio is likely to be less than unity. Recent studies show that steady state values of about 0.1 are reached after $\sim 10^5$ yr if the gas density is 10^5 cm^{-3} or higher. Lower densities implies a higher $[\text{H}_3^+]/[\text{HCO}^+]$ ratio (which is approximately inversely proportional to the square root of n_{H}) and a stronger time dependence. This abundance ratio introduces a severe limitation to the derived fractional electron abundances, $\chi(e^-)$, since $\chi(e^-) \sim \chi(\text{H}_3^+)/\chi(\text{HCO}^+) \cdot 10^{-7}$ (Eq. A10).

2) The cosmic ray ionization rate of molecular hydrogen, ζ , lies in the range $10^{-18} - 10^{-16} \text{ s}^{-1}$ (see Sect. A.2). Whatever value is adopted, it probably remains constant within the studied region since the projected distance between the NW and SE end of the R CrA core is only 0.4 pc.

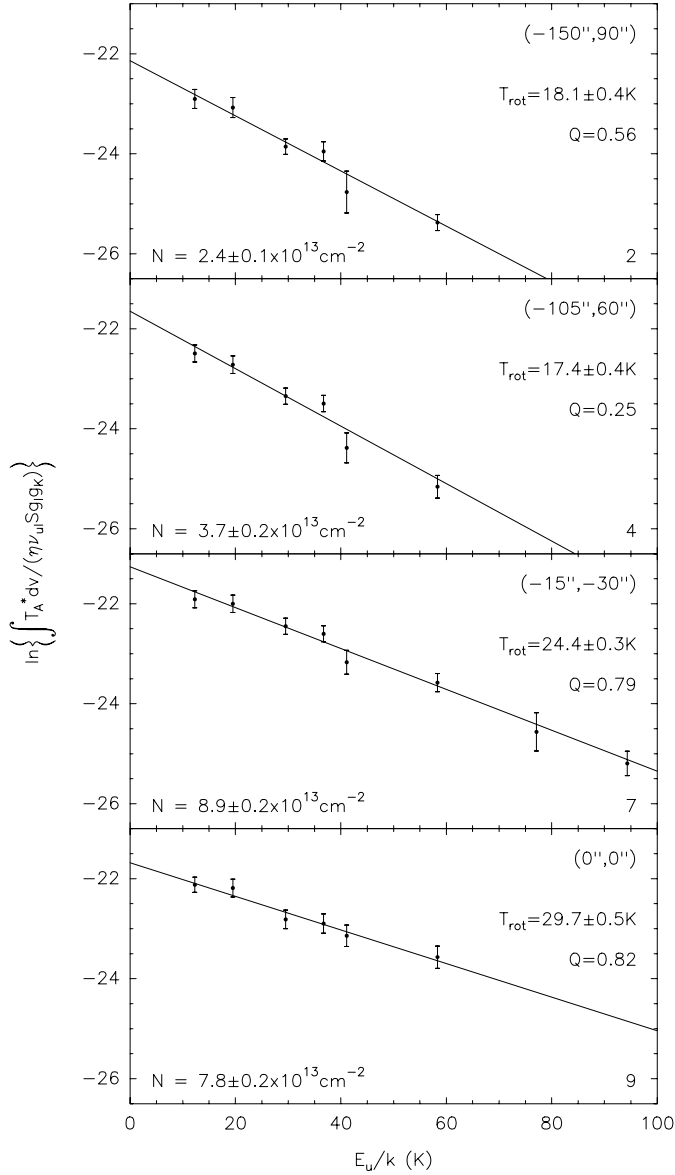


Fig. 7. Rotational diagrams of the CH₃CCH spectra towards positions 2, 4, 7 and 9. The lines represent linear least-squares fits to the data. The rotational temperature (T_{rot}) and the ‘Q-value’ derived from each fit are given in the top right of each panel. The total CH₃CCH column density (N) is given in the bottom left of each panel.

3) The combined fractional abundance of neutral atoms and molecules other than H₂ (i.e. $\chi(\text{CO}) + \chi(\text{O}) + \chi(\text{C}) + \chi(\text{N}_2) + \chi(\text{HD}) + \dots$) is likely to be lower than $4.0 \cdot 10^{-4}$ (Lee et al. 1996, CWTH). Hereafter we denote this combined fractional abundance of neutrals *including* CO by $\chi(\mathcal{N}')$, distinct from $\chi(\mathcal{N})$ introduced in Sect. A.2.

4) The combined fractional abundance of HD and D, $\chi(\text{HD}) + \chi(\text{D})$, is between $1.65 \cdot 10^{-5}$ and $3.3 \cdot 10^{-5}$ (see Sect. A.2).

One further constraint is the number density of molecular hydrogen, n_{H_2} , which determines the ratio between the fractional electron abundance and the cosmic ray ionization rate.

We have estimated the gas densities towards selected positions from the observed DCO⁺ ($J = 2 - 1$) and ($J = 3 - 2$) line by using the Monte Carlo radiative transfer simulation program of M. Juvela (Juvela 1997). The model cloud was assumed to be a microturbulent homogenous sphere with a diameter of 30'' (as seen from a distance of 130 pc). The collisional rate coefficients were adopted from Monteiro (1985). The adopted excitation temperatures for C¹⁸O listed in Table 3 were used as kinetic temperature estimates. The fact that the $J = 3 - 2$ lines are relatively strong (the ($J = 3 - 2$)/($J = 2 - 1$) ratio ranges from 0.5 to 0.9) implies high densities: the derived values lie in the range $1 - 3 \cdot 10^6 \text{ cm}^{-3}$, except for position 7 (the dense clump near IRS 7), where the intensity ratio ($J = 3 - 2$)/($J = 2 - 1$) is almost unity. This ratio suggests a very high density ($\sim 5 \cdot 10^6 \text{ cm}^{-3}$ or larger), but its value is also very uncertain, and higher transitions should be observed to determine the density more accurately. In the following we assume that the characteristic density towards the selected positions (corresponding to the H¹³CO⁺ and DCO⁺ emission peaks) is 10^6 cm^{-3} .

The solution for the parameters was obtained by fixing the fractional electron density towards position 12 such that the ratio $\chi(\text{H}_3^+)/\chi(\text{HCO}^+)$ is of order 0.1 at all 12 selected locations. This ratio was allowed vary since chemistry models (e.g. Lee et al 1996, Smith et al. 1994) indicate that it should. The adopted value for $\chi(e^-)$ at location 12 is $2 \cdot 10^{-8}$. The requirements presented in items 3) and 4) above imply then that the ratio ζ/n_{H_2} is about $10^{-22} \text{ s}^{-1} \text{ cm}^3$ which, with the assumed density, corresponds to an ionization rate of 10^{-16} s^{-1} .

Substitution of the adopted value of $\chi(e^-)$ into Eq. (A10) gives an estimate for $\chi(\text{H}_3^+)$ at location 12, which can be further substituted into Eq. (A27) to obtain a value for $[\text{H}_2\text{D}^+]/[\text{H}_3^+] \equiv R$. Eq. (A18), along with the assumed value of ζ/n_{H_2} , can be used for deriving an estimate for the destruction rate, δ' , of H₃⁺ in reactions with neutral species (see Sect. A.2). Finally, Eq. (A19) gives an estimate for the neutral destruction rate, δ , of H₂D⁺, which together with the derived value of δ' implies, by Eq. (A20), that the combined fractional abundance of HD and D towards position 12 is $1.8 \cdot 10^{-5}$. A higher fractional abundance would lead to unrealistically large abundances of neutral species towards some locations (constraint 3).

Towards positions with temperature estimates (i.e. 2, 4, 7 and 9) and the two remaining positions in the southeastern core (10 and 11), where the temperature is assumed to be 13 K, the quantities $[\text{H}_2\text{D}^+]/[\text{H}_3^+]$, $\chi(e^-)$, δ , δ' and $\chi(\text{H}_3^+)$ have been solved by iteration. First, the ratio $[\text{H}_2\text{D}^+]/[\text{H}_3^+] (\equiv R)$ has been solved from Eq. (A27) assuming that the $[\text{H}_3^+]/[\text{HCO}^+]$ ratio is the same as for position 12. Thereafter $\chi(e^-)$ has been solved from Eq. (A10). The destruction rates δ and δ' have been derived from Eqs. (A19) and (A20), and finally, an estimate for $\chi(\text{H}_3^+)$ has been obtained from Eq. (A18), which has been again substituted into Eq. (A27) to get a *new* value for R , and the process repeated. The fractional deuterium abundance, $\chi(\text{D})$, was solved from Eq. (A25), and the fractional abundance of neutrals destroying H₃⁺ and H₂D⁺ ions, $\chi(\mathcal{N}')$, has been derived from Eq. (A16) by assuming that the rate coefficient k for all such reactions is $1.5 \cdot 10^{-9} \text{ cm}^3 \text{ s}^{-1}$.

In this calculation we have assumed that $n_{\text{H}_2} = 10^6 \text{ cm}^{-3}$, $\zeta = 10^{-16} \text{ s}^{-1}$ and $\chi(\text{HD}) + \chi(\text{D}) = 1.8 \cdot 10^{-5}$ are valid throughout the cloud. The last assumption, i.e. $\chi(\text{HD}) + \chi(\text{D}) \sim \text{constant}$, is based on the chemistry models of Brown & Rice (1986) and Brown & Millar (1989) according to which the fractional HD abundance varies little compared with other deuterated species. Our results indicate that the fractional D abundance is much smaller than that of HD and its variation has, therefore, little effect on the combined abundance.

The derived parameters are listed in Columns (8), (9), (10), (11) and (12) of Table 4. Towards position 9 (0,0) the estimates for the parameters in Columns (8) to (12) failed since the DCO⁺/HCO⁺ ratio is slightly too *high* for the derived kinetic temperature (the equilibrium constant $K^{-1}(T) \equiv k_-/k_+$ of the reaction $\text{H}_3^+ + \text{HD} \rightleftharpoons \text{H}_2\text{D}^+ + \text{H}_2$ should bring this ratio down in warm conditions). Therefore only upper limits for the $[\text{H}_2\text{D}^+]/[\text{H}_3^+]$ ratio and $\chi(e^-)$ derived from Eqs. (A8) and (A11) are indicated. The elevated level of deuterium fractionation towards IRS 7 may be attributable to the protostar's cool envelope: If the envelope contributes more strongly to the low rotational transitions of DCO⁺ and H¹³CO⁺ than to the methylacetylene emission used in the determination of the kinetic temperature then a 'high' level of deuterium fractionation will be observed (see Wootten & Shah 1998).

Besides the variation in the DCO⁺/HCO⁺ ratio in Table 4, the following tendencies can be discerned:

1) The derived $[\text{H}_2\text{D}^+]/[\text{H}_3^+]$ ratio is approximately three times the $[\text{DCO}^+]/[\text{HCO}^+]$ ratio. As discussed in Appendix A this is due to the adopted rate at which deuterium atoms are removed by collisions with grains.

2) The $[\text{H}_3^+]/[\text{HCO}^+]$ ratios lie between 0.06 and 0.2, being lowest near IRS 7. The fractional H₃⁺ abundance increases from about $2 \cdot 10^{-10}$ towards position 7 to $5 \cdot 10^{-10}$ towards position 12. These abundances agree rather well with the model results of Lee et al. (1996). Likewise, the fractional electron abundance, $\chi(e^-)$, increases from $0.6 \cdot 10^{-8}$ near IRS 7 to $2 \cdot 10^{-8}$ in the southeastern clump. This reflects the increase in the $[\text{H}_3^+]/[\text{HCO}^+]$ ratio (see Eq. A10) and the decrease in the $[\text{HCO}^+]/[\text{CO}]$ ratio (Eq. A21) with distance from IRS 7.

3) The derived fractional abundances of deuterium atoms, $\chi(\text{D})$ and other neutral species, $\chi(\mathcal{N}')$, vary markedly, the former increasing and the latter decreasing as a function of projected distance from IRS 7. The destruction rate of H₃⁺ in the reactions with neutrals, δ' (corresponding to $\chi(\mathcal{N}')$) is $4.2 \cdot 10^{-13} - 5.8 \cdot 10^{-13} \text{ cm}^3\text{s}^{-1}$ in the northwestern clump, and $2.6 \cdot 10^{-13} - 3.5 \cdot 10^{-13} \text{ cm}^3\text{s}^{-1}$ in the southeastern clump.

It should be noted that the value of the electron abundance towards position 12 was chosen somewhat arbitrarily based on the predictions of earlier chemistry models. The derived values of $\chi(e^-)$ and $\chi(\text{H}_3^+)/\chi(\text{HCO}^+)$ towards other positions are proportional to this value. The cosmic ray ionization should be adjusted accordingly in order to keep the abundances of neutrals within reasonable limits. This would, however, have little effect on the relative abundances towards selected positions. Therefore we believe that the numbers listed in Table 4 indicate the true abundance variations within the cloud.

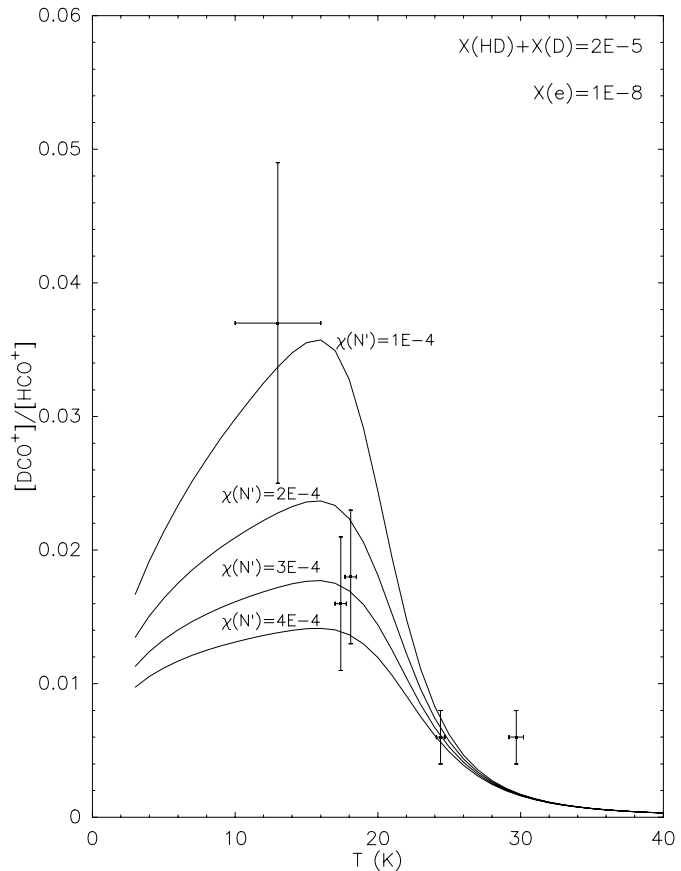


Fig. 8. The DCO⁺/HCO⁺ abundance ratio as a function of kinetic temperature as predicted by a simplified chemistry model (see text). The quantity $\chi(\mathcal{N}')$ denotes the fractional abundance of neutral species other than H₂ (i.e. CO, O, C, HD, N₂, CH₄, N, H₂O,...) taking part in the destruction of H₃⁺ and H₂D⁺ ions. The reaction rate constants adopted are from Lee et al. (1996). The observed DCO⁺/HCO⁺ ratios and their error are also indicated. For the left-most data point, the temperature is assumed.

The variation of the DCO⁺/HCO⁺ ratio as a function of the kinetic temperature is predicted by chemical theory. This variation occurs via the rate constants involved in the destruction of H₂D⁺, in particular the equilibrium constant $K^{-1}(T)$ (Herbst 1982). In Fig. 8 the dependence, as derived from Eqs. (A7) and (A19), is graphed for the simplified case where atomic deuterium has been omitted, which implies that the DCO⁺/HCO⁺ ratio is about one third of the H₂D⁺/H₃⁺ ratio. The DCO⁺/HCO⁺ ratio is indicated for four values of $\chi(\mathcal{N}')$, i.e. $1 \cdot 10^{-4}$, $2 \cdot 10^{-4}$, $3 \cdot 10^{-4}$ and $4 \cdot 10^{-4}$. The fractional abundances $\chi(\text{HD}) + \chi(\text{D})$ and $\chi(e^-)$ are assumed to be $2 \cdot 10^{-5}$, and $1 \cdot 10^{-8}$, respectively. A higher fractional electron abundance would decrease the DCO⁺/HCO⁺ ratios for a particular value of $\chi(\mathcal{N}')$.

At low temperatures where $K^{-1}(T)$ is very small, the DCO⁺/HCO⁺ ratio is governed by the fractional abundances of electrons, $\chi(e^-)$, and neutral species, $\chi(\mathcal{N}')$. The decrease towards the lowest temperatures is mainly due to the temperature dependence of the rate coefficient for the proton transfer reaction

Table 4. Chemical data towards 12 selected positions. The column density ratios DCO⁺/HCO⁺ (3) and HCO⁺/CO (4), the fractional HCO⁺ abundance (5), the Gaussian half power widths of the DCO⁺ ($J = 2 - 1$) lines (6) and the rotational temperatures for CH₃CCH (7) have been derived directly from observations, whereas the abundance ratios H₂D⁺/H₃⁺ (8) and H₃⁺/HCO⁺ (9) and the fractional abundances $\chi(e^-)$ (10), $\chi(D)$ (11) and $\chi(\mathcal{N}')$ (12) were derived using the chemistry model described in Appendix A. For the data presented here it has been assumed that the cosmic ionization rate $\zeta = 10^{-16} \text{ s}^{-1}$, the combined fractional abundance $\chi(\text{HD}) + \chi(D) = 1.8 \cdot 10^{-5}$ and the number density $n_{\text{H}_2} = 10^6 \text{ cm}^{-3}$.

(1) No.	(2) $\Delta\alpha$ (")	(2) $\Delta\delta$ (")	(3) $\frac{[\text{DCO}^+]}{[\text{HCO}^+]}$	(4) $\frac{[\text{HCO}^+]}{[\text{CO}]}$ $\cdot 10^5$	(5) $\chi(\text{HCO}^+)$ $\cdot 10^9$	(6) Δv DCO ⁺ (kms ⁻¹)	(7) T_{rot} CH ₃ CCH (K)	(8) $\frac{[\text{H}_2\text{D}^+]}{[\text{H}_3^+]}$	(9) $\frac{[\text{H}_3^+]}{[\text{HCO}^+]}$ *	(10) $\chi(e^-)$ $\cdot 10^8$	(11) $\chi(D)$ $\cdot 10^8$	(12) $\chi(\mathcal{N}')$ $\cdot 10^4$
1	-210	210	0.018±0.006	1.9±0.5	1.5±0.6	0.89±0.02						
2	-150	90	0.018±0.005	2.7±0.6	2.2±0.7	1.14±0.01	18.1±0.4	0.050	0.09	1.1	1.2	2.5
3	-105	-45	0.014±0.004	3.1±0.8	2.3±0.9	1.00±0.03						
4	-105	60	0.016±0.005	3.9±0.9	3.1±1.1	1.32±0.02	17.4±0.4	0.044	0.06	0.6	0.8	3.2
5	-75	30	0.009±0.003	4.7±1.1	3.7±1.3	1.62±0.03						
6	-60	-15	0.007±0.002	4.6±1.1	3.6±1.3	1.18±0.03						
7	-15	-30	0.006±0.002	3.5±0.8	2.9±0.9	0.98±0.01	24.4±0.3	0.016	0.08	1.0	0.4	2.2
8	0	-210	0.027±0.009	2.5±0.7	1.8±0.8	1.01±0.01						
9	0	0	0.006±0.002	2.3±0.5	1.9±0.6	1.53±0.03	29.7±0.5	< 0.017	-	< 1.6	-	-
10	150	-180	0.035±0.011	2.8±0.8	2.0±0.9	0.78±0.01		0.100*	0.17*	1.7*	4.3*	1.0*
11	210	-195	0.028±0.008	3.3±0.8	2.4±1.0	0.85±0.01		0.080*	0.12*	1.1*	2.7*	1.4*
12	240	-255	0.037±0.012	2.5±0.7	1.8±0.8	0.83±0.01		0.110*	0.20*	2.0*	4.9*	0.9*

* assuming that $T_{\text{kin}} = 13 \text{ K}$

given by reaction 2 in Table A.1. The use of a temperature independent rate constant for this reaction (e.g. $1.7 \cdot 10^{-9} \text{ cm}^3 \text{ s}^{-1}$ as used in several previous studies) would make the DCO⁺/HCO⁺ ratio higher for a particular value of $\chi(\mathcal{N}')$ and the curves would be almost flat below 16 K. At high temperatures, $K^{-1}(T)$ dominates the denominator of Eq. A18 and draws the DCO⁺/HCO⁺ ratio down. Between 16 and 30 K, where $K^{-1}(T) \sim \chi(\mathcal{N}')$, the ratio has a very steep temperature dependence. Also indicated in Fig. 8 are the DCO⁺/HCO⁺ ratios and their errors as derived from the observations for the four locations where the temperature has been determined and for position 12, where the temperature is assumed to be $13 \pm 3 \text{ K}$. It can be seen that relatively high abundances of the neutral species \mathcal{N}' are required in positions 2 and 4 in the northwestern clump with ratios slightly below 0.02. In contrast, the high DCO⁺/HCO⁺ ratios in the southeastern clump (positions 10, 11 and 12) would, according to this model, require low values of $\chi(\mathcal{N}')$. This is also evident in the numerical results presented in Table 4.

5. Discussion

5.1. Deuterium fractionation

The derived DCO⁺/HCO⁺ abundance ratios show an overall tendency to increase with angular separation from IRS 7, the centre of the current star formation activity in the cloud. The values near IRS 7 are characteristic for warm clouds with embedded infrared sources whereas in the southeastern clump the ratios reach typical dark cloud values (e.g. Wootten et al. 1982, Williams et al. 1998).

According to the discussion in the previous section, the temperature changes via the equilibrium constant $K(T)$ alone can-

not explain the variation of the deuterium fractionation rate. Although both northwestern and southeastern clumps are cool, the deuterium fractionation rates in these two locations are surprisingly different. The simple chemistry model outlined in Appendix A suggests that the difference is due to the variation in the abundances of the species destroying the H₃⁺ and H₂D⁺ ions. These destructive agents can be either electrons or various neutral species reacting with the aforementioned ions. As indicated by the variation of the HCO⁺/CO ratio, the fractional electron abundance does change over the mapped region but this occurs roughly in step with the DCO⁺/HCO⁺ abundance ratio. Furthermore, the derived fractional electron abundances are very low, i.e. of order $1 \cdot 10^{-8}$. Therefore, the most likely explanation for the difference in the DCO⁺ fractionation between the northwestern and southeastern clumps is a variation of the abundances of *neutral* species destroying the H₃⁺ and H₂D⁺ ions.

The H₃⁺ and H₂D⁺ ions rapidly give up one proton to any atom or molecule that has a proton affinity greater than that of H₂ (Smith et al. 1994). This reaction has the generic form $\text{H}_3^+ + \text{X} \rightarrow \text{XH}^+ + \text{H}_2$. CWTH point out that according to chemistry models atomic oxygen and CO are by far the most abundant of such species. Also N₂, which reaches a high relative abundance at steady state ($\chi \sim 10^{-5}$, CWTH) reacts willingly with H₃⁺. The reaction with molecular oxygen, O₂, which has a similar steady state abundance as N₂, occurs slowly and probably has a minor effect on the deuterium fractionation.

In CWTH the abundance variation of neutral species is suggested to be due to their depletion onto dust grain surfaces. This process is described by the depletion factor f_D with respect to the gas phase elemental abundances adopted or derived

in chemistry models (e.g. Lee et al. 1996). Without desorption mechanisms which release molecules from the grain mantles, the degree of depletion should increase with time. Since it is not likely that the NW clump would represent an earlier stage of evolution than the SE clump, a natural assumption is that either desorption mechanisms or mechanisms that prevent gas from condensing are working more efficiently in the northwestern part of the R CrA core. The elevated gas kinetic temperature of the NW clump and its proximity to an active star forming region suggest that desorption mechanisms are indeed efficient there. The embedded infrared sources of the ‘Coronet’ cluster heat the dust and probably cause enhanced turbulence through their stellar winds (e.g. Wilking et al. 1985, Wilking et al. 1997). The visually bright Herbig Ae/Be stars TY CrA and HD176386, which illuminate the reflection nebula NGC 6726/7 in front of the northwestern clump (Graham 1991), likely give rise to an intensified UV radiation field impinging on the cloud.

According to Charnley (1997) a modest warming of the dust grains will lead to thermal evaporation of the most volatile molecules (H₂, CO, O₂ and N₂) which then affect the DCO⁺/HCO⁺ abundance ratio. Furthermore, increased turbulence in dense gas causes frequent grain-grain collisions, which can provoke mantle explosions due to frozen radicals (d’Hendecourt et al. 1982; d’Hendecourt et al. 1985; Tielens & Allamandola 1987; Shalabiea & Greenberg 1994). The DCO⁺ linewidths are larger in the NW clump (1.1 – 1.6 km s⁻¹) than those in the SE clump (0.8 – 0.9 km s⁻¹, see Table 4). The collision velocity between grains is also probably slightly higher in the former clump. It should be noted that the DCO⁺ linewidths are not higher in the neighbourhood of IRS 7 (positions 6, 7 and 9) than in the NW clump. However, towards IRS 7 (position 9) where the DCO⁺/HCO⁺ ratio is lowest, the dust temperature is probably sufficient for rapid diffusion of radicals over the grain surface, which can lead to efficient mantle ejection (d’Hendecourt et al. 1982).

An alternative to desorption as a factor reducing the degree of deuteration is the enhancement of non-thermal reactions (e.g. the reverse of reaction 8 in Table A.1) occurring in magnetohydrodynamic waves caused by perturbations in weakly ionized gas as presented by Charnley & Roberge (1992). This model predicts that the degree of deuterium fractionation should be highest in the molecular gas with the narrowest linewidths. Also turbulent mixing of material between the inner and outer layers of a cloud, which according to Xie et al. (1995) may sustain large C and C⁺ abundances even in the interiors of dense cores, can have a similar effect. According to the latter model the C/CO ratio depends on the typical velocity and the length scale of the turbulence, and may therefore be correlated with the line widths. Although observations towards the SE clump seem to support these ideas, the relation between the DCO⁺/HCO⁺ ratio and the linewidth is not straightforward as discussed above. Also CWTB found very weak correlation between the linewidths and the degree of deuterium fractionation. Furthermore, in the model of Xie et al. (1995) the chemical composition is modified via transporting electrons and ions from the cloud surface and therefore the enhanced abundance of C atoms should be accom-

panied with a higher electron abundance. In our data there is, however, little evidence for an increased electron density in the regions where the deuterium fractionation ratio is lowest.

5.2. The degree of ionization

The fractional electron abundance, $\chi(e^-)$, is larger in the quiescent southeastern clump than in the neighbourhood of the active region. This is reflected in the observed decrease of the [HCO⁺]/[CO] ratio with the distance from IRS 7. Given that CO is actually depleted by about a factor of two in the southeastern clump, the decrease of the [HCO⁺]/[CO] ratio towards this region can only be attributed to a decrease in the HCO⁺ fractional abundance, probably caused by an enhanced electron recombination rate. However, uncertainties related to the observed abundances and abundance ratios (see Table 4) do not allow us to build a simple relation between the [HCO⁺]/[CO] ratio and $\chi(e^-)$. Measurements of DCO⁺ and temperature estimates are also needed to determine $\chi(e^-)$ more precisely in cloud cores, as already stated by CWTB. We found higher electron fractions in those regions where depletion of neutral species is higher. The reason for this tendency is mostly due to the fact that H₃⁺ tends to increase with depletion because its destruction rate decreases proportionally. However, the HCO⁺ formation is little affected since the effect of an increase in H₃⁺ abundance is largely nullified by a decrease in $\chi(\text{CO})$. The net result is a higher [H₃⁺]/[HCO⁺] abundance ratio or, equivalently, a higher $\chi(e^-)$.

As discussed in Sect. 3.4, the fractional abundances of CO, $\chi(\text{CO})$, derived from a linear relation between the C¹⁸O column density and the colour excess $E(J - K)$ (Harjunpää & Mattila 1996) are valid only towards four positions in the southeastern part of the R CrA core. Elsewhere the values of $\chi(\text{CO})$ are derived from the extrapolation of the aforementioned relation. These fractional abundances are needed for estimates of $\chi(\text{HCO}^+)$ and, according to our test calculations, primarily affect the derived electron abundances, $\chi(e^-)$. If $\chi(\text{CO})$ is in reality smaller than estimated by a factor of two, say, towards the northwestern clump (i.e. CO is depleted to a greater extent), the derived values of $\chi(e^-)$ become equal to those in the southeastern clump, and the spatial gradient in the electron abundance disappears. On the basis of the discussion above, a more likely alternative is that the CO abundance is larger in the northwest. In this case the derived electron abundances will be smaller by an amount roughly proportional to $\chi(\text{CO})$.

The fact that C¹⁸O may be tracing lower density regions than DCO⁺ and H¹³CO⁺ produces another source of uncertainty in the derived abundances. Depending on the cloud’s density structure the HCO⁺/CO abundance ratios are likely to be lower limits. Correcting for this would further lower the fractional electron abundances (see Eq. A10). However, at the level of ionization deduced for the R CrA core, changing $\chi(\text{CO})$ or [HCO⁺]/[CO] would not alter the derived neutral abundances $\chi(\mathcal{N}')$ significantly.

6. Conclusions

We have observed the variation of the DCO⁺/HCO⁺ abundance ratio over the R CrA cloud core. The ratio ranges from 0.006 to 0.04, being lowest towards two locations near the embedded infrared source IRS 7 where the kinetic temperature is 24 – 30 K. The difference in the DCO⁺/HCO⁺ ratio between two separate clumps within the core (which we have called the “north-western” and “southeastern” clumps) cannot be explained by the temperature difference alone, but in conjunction with the supposition that the fractional abundance of neutral species is larger in the northwestern clump. This increase is probably due to enhanced desorption from grain surfaces arising from star formation activity in the vicinity. The fractional D abundance is anticorrelated with the combined abundance of neutral species (CO, O, N₂, etc.) which take part in the destruction of the H₃⁺ and H₂D⁺ ions. This behaviour is in accordance with the results of chemical models including accretion on grain surfaces (Brown & Millar 1989).

The electron fraction $\chi(e^-)$ has been estimated from a simple chemical model where neutral species (besides CO) destroy H₃⁺ and H₂D⁺ and reactions with atomic deuterium are included. We found that the $\chi(e^-)$ is larger in the quiescent southeastern clump than nearby the active star forming region. This gradient in the electron fraction is detectable through the observation of the [HCO⁺]/[CO] abundance ratio, which tends to decrease with increasing $\chi(e^-)$. Finally, higher gas phase depletion implies a higher degree of ionization. An accurate measurement of $\chi(e^-)$ therefore requires estimates of the amount of depletion as well as of the gas temperature and volume density.

The average H¹³CO⁺/HC¹⁸O⁺ abundance ratio in the R CrA core is 10.5 ± 2.2 , whereas the average ¹³C/¹²C abundance ratio towards the core has been found to be 9.2 ± 1.3 (Harjunpää & Mattila 1996). This agreement supports the prediction of chemistry models that predict that the main formation channel of HCO⁺ is the direct protonation of CO. It also emphasizes the fact that the degree of ¹³C fractionation should be determined when H¹³CO⁺ is used for HCO⁺ column density estimates.

Further examination of the influence of various possible processes on the chemical composition of the R CrA core would be aided by an accurate temperature measurements in the southeastern clump where the DCO⁺/HCO⁺ ratio is large. A search for direct evidence of effective desorption mechanisms near IRS 7 and the northwestern clump may also yield useful information on the chemical composition of the core. Species like NaOH (Tielens & Allamandola 1987) and D₂CO (Ceccarelli et al. 1998) which probably only form on grain surfaces, would be well suited for such a survey. Moreover, the high abundance of atomic oxygen predicted by simple chemical considerations could possibly be traced by the far-infrared fine-structure lines of OI.

Acknowledgements. We are grateful to Mika Juvela for use of his Monte Carlo program. We thank Arto Heikkilä, Malcolm Walmsley and the referee, Al Wootten, for helpful comments on the manuscript. The work by I.M.A. and J.H. has been supported by the Finnish Academy

through grant No. 1011055. P.C. acknowledges partial support from the ASI through grant ARS-96-66, and from CNR through grants 96/00317 and 97.00018.CT02. The Swedish-ESO Submillimetre Telescope is operated jointly by ESO and the Swedish National Facility for Radio Astronomy, Onsala Space Observatory at Chalmers University of Technology.

Appendix A: deuterium fractionation in the formyl ion

In the following we outline the DCO⁺ - HCO⁺ chemistry model and detail the method used for determining the electron abundance from the observed abundances of HCO⁺, DCO⁺ and CO. The basis for the model is the theory of Dalgarno & Lepp (1984, hereafter DL), which involves atomic deuterium, with modifications to accommodate more recently determined electron recombination rates for H₃⁺ and H₂D⁺ (Sundström et al. 1994, Larsson et al. 1996). The leading reactions and their rate constants are listed in Table A.1.

A.1. Production and destruction of DCO⁺ and HCO⁺ and the electron density

The main formation channel of HCO⁺ is proton transfer from H₃⁺ to CO (reaction 1 in Table A.1). The production of DCO⁺ is assumed to proceed primarily through reactions 2 and 3 in Table A.1. In reaction 2, the branching ratio 2 : 1 in favour of the formation of HCO⁺ reflects the isotopic ratios in the H₂D⁺ ion. Chin et al. (1996) estimated that the contribution of reaction 3 to the formation of DCO⁺ increases from 36% to 56% when the temperature rises from 10 to 30 K. In early deuterium fractionation studies (e.g. Guélin et al. 1977, 1982; Wootten et al. 1979, 1982) reaction 3 was neglected because of the assumed low abundance of D atoms in dense gas. Both HCO⁺ and DCO⁺ are destroyed in recombination reactions with electrons (reactions 4 and 5 in Table A.1).

Assuming that reactions 1–5 dominate the formation and destruction of DCO⁺ and HCO⁺, one obtains the following equilibrium conditions:

$$\frac{2}{3}k_2[\text{H}_2\text{D}^+][\text{CO}] + k_1[\text{H}_3^+][\text{CO}] = \alpha_4[e^-][\text{HCO}^+] + k_3[\text{D}][\text{HCO}^+] \quad (\text{A1})$$

$$\frac{1}{3}k_2[\text{H}_2\text{D}^+][\text{CO}] + k_3[\text{D}][\text{HCO}^+] = \alpha_5[e^-][\text{DCO}^+], \quad (\text{A2})$$

where [] denotes the abundance or number density in cm⁻³. By dividing these equations one arrives at the following equilibrium DCO⁺/HCO⁺ abundance ratio (DL, Eq. (14)):

$$\frac{\alpha_5}{\alpha_4} \frac{[\text{DCO}^+]}{[\text{HCO}^+]} = \frac{\frac{1}{3}k_2[\text{H}_2\text{D}^+][\text{CO}] + k_3[\text{D}][\text{HCO}^+]}{k_1[\text{H}_3^+][\text{CO}] + \frac{2}{3}k_2[\text{H}_2\text{D}^+][\text{CO}] - k_3[\text{D}][\text{HCO}^+]}. \quad (\text{A3})$$

To facilitate the solution of forthcoming equations we adopt the following definitions of DL:

$$r \equiv \frac{[\text{DCO}^+]}{[\text{HCO}^+]} \quad \text{and} \quad R \equiv \frac{[\text{H}_2\text{D}^+]}{[\text{H}_3^+]}. \quad (\text{A4})$$

Table A1. Principal reactions of the DCO⁺ - HCO⁺ chemistry

No.	Reaction	Rate coefficient* (cm ³ s ⁻¹)
1	H ₃ ⁺ + CO $\xrightarrow{k_1}$ HCO ⁺ + H ₂	$k_1 = 6.2 \cdot 10^{-10} (300/T)^{0.5}$
2	H ₂ D ⁺ + CO $\xrightarrow{k_2}$ HCO ⁺ + HD [67%] DCO ⁺ + H ₂ [33%]	$k_2 = 6.2 \cdot 10^{-10} (300/T)^{0.5}$
3	HCO ⁺ + D $\xrightarrow{k_3}$ H + DCO ⁺	$k_3 = 1.0 \cdot 10^{-9}$
4	HCO ⁺ + e ⁻ $\xrightarrow{\alpha_4}$ H + CO	$\alpha_4 = 2.0 \cdot 10^{-7} (300/T)^{0.75}$
5	DCO ⁺ + e ⁻ $\xrightarrow{\alpha_5}$ D + CO	$\alpha_5 = 2.0 \cdot 10^{-7} (300/T)^{0.75}$
6	H ₃ ⁺ + e ⁻ $\xrightarrow{\alpha_6}$ H ₂ + H [25%] H + H + H [75%]	$\alpha_6 = 1.15 \cdot 10^{-7} (300/T)^{0.65}$
7	H ₂ D ⁺ + e ⁻ $\xrightarrow{\alpha_7}$ H + H + D [73%] HD + H [20%] H ₂ + D [7%]	$\alpha_7 = 6 \cdot 10^{-8} (300/T)^{0.65}$
8	H ₃ ⁺ + HD $\xrightleftharpoons[k_-]{k_+}$ H ₂ D ⁺ + H ₂	$k_+ = 1.5 \cdot 10^{-9}$ $k_- = 2.0 \cdot 10^{-9} (300/T)^{0.8} \exp(-230/T)$
9	H ₃ ⁺ + D $\xrightarrow{k_9}$ H ₂ D ⁺ + H	$k_9 = 1.0 \cdot 10^{-9}$
10	H ₂ ⁺ + H ₂ $\xrightarrow{k_{10}}$ H ₃ ⁺ + H	$k_{10} = 1 \cdot 10^{-9}$

* The reaction rates are adopted from Lee et al. (1996) and from CWTH (for reactions involving deuterium).

Furthermore, we define ξ by

$$\xi \equiv \frac{k_3}{k_1} \frac{[\text{D}]}{[\text{CO}]} \frac{[\text{HCO}^+]}{[\text{H}_3^+]}. \quad (\text{A5})$$

By dividing the numerator and denominator of the right hand side of Eq. A3 by $k_1[\text{H}_3^+][\text{CO}]$ and using the above defined notation, Eq. A3 can be expressed as

$$\frac{\alpha_5}{\alpha_4} r = \frac{\frac{1}{3} \frac{k_2}{k_1} R + \xi}{\frac{2}{3} \frac{k_2}{k_1} R + 1 - \xi}. \quad (\text{A6})$$

Substituting the rate coefficients adopted from Lee et al. (1996) (i.e. $k_2 = k_1$ and $\alpha_5 = \alpha_4$) into Eq. A6 leads to

$$R = \frac{3[r - (1+r)\xi]}{1 - 2r}. \quad (\text{A7})$$

The term ξ represents the contribution attributable to free deuterium atoms. This contribution, the size of which is essentially determined by the abundance ratio $[\text{D}]/[\text{e}^-]$ (see below), is not negligible. If this term is omitted, however, it can be seen that $R \approx 3r$. This approximation has been frequently used in earlier studies (e.g. Guélin et al. 1982). The requirement that ξ be equal to or greater than zero gives an upper limit for R :

$$R \leq \frac{3r}{1 - 2r}. \quad (\text{A8})$$

The electron density, $[e^-]$, can be derived from Eq. A1:

$$[e^-] = \frac{k_1}{\alpha_4} \frac{[\text{H}_3^+]}{[\text{HCO}^+]} [\text{CO}] \left\{ 1 + \frac{2}{3} \frac{k_2}{k_1} R - \xi \right\}. \quad (\text{A9})$$

This method of estimating the electron abundance, starting from the equilibrium equation for HCO⁺, was first used by Wootten et

al. (1979). The transformation to fractional abundances relative to molecular hydrogen, χ , can be made by dividing both sides by $[\text{H}_2]$. Furthermore, substitution of the solution for ξ from Eq. A7 into Eq. A9 gives the following formula for the fractional electron density:

$$\chi(e^-) = \frac{k_1}{\alpha_4} \frac{\chi(\text{CO})}{\chi(\text{HCO}^+)} \chi(\text{H}_3^+) \frac{1 + R}{1 + r}. \quad (\text{A10})$$

With the aid of Eq. A8, one can then obtain the following upper limit for the fractional electron abundance:

$$\chi(e^-) \leq \frac{k_1}{\alpha_4} \frac{\chi(\text{H}_3^+)}{\chi(\text{HCO}^+)} \frac{\chi(\text{CO})}{1 - 2r}. \quad (\text{A11})$$

The explicit temperature dependence of the fractional electron abundance is rather weak. From the rate constants given in Table A.1, $k_1/\alpha_4 = 1.3 \cdot 10^{-3} (T/10\text{K})^{0.25}$. The fractional CO abundance, $\chi(\text{CO})$, is usually found to be of order $1 \cdot 10^{-4}$. This is also the case in CrA (Harjunpää & Mattila 1996). The product $k_1/\alpha_4 \chi(\text{CO})$ is, under typical dark cloud conditions, of the order 10^{-7} . Since r and R are both small, the term including them on the right hand side of Eq. A10 is always close to unity. In the locations examined in the present study, $\chi(\text{HCO}^+)$ varies from $1.5 \cdot 10^{-9}$ to $3.7 \cdot 10^{-9}$. According to the time-dependent chemical model calculations of Smith et al. (1994) for dense molecular clouds, the higher values correspond to abundances at an early stage of chemical evolution. Smith et al. (1994) furthermore predict that the fractional H₃⁺ abundance, $\chi(\text{H}_3^+)$, lies in the range $2 - 4 \cdot 10^{-9}$ so that the ratio $\chi(\text{H}_3^+)/\chi(\text{HCO}^+)$ decreases with time from 0.9 to 0.3. Lee et al. (1996) derive considerably lower values for this ratio. In their standard model for $T = 10$ K, $n_H = 10^4 \text{ cm}^{-3}$, conditions which correspond to those in Smith et al. (1994), the ratio $\chi(\text{H}_3^+)/\chi(\text{HCO}^+)$ decreases from

0.6 to 0.2, the latter number representing steady state. As explained in Sect. 4.2, recent gas phase chemical models predict a ratio of about 0.1 when $n_{\text{H}_2} = 10^5 \text{ cm}^{-3}$. This ratio turned out to be roughly inversely proportional to the square root of the density. Thus, depending on the adopted $\text{H}_3^+/\text{HCO}^+$ ratio, the fractional electron abundance is of the order $10^{-8} - 10^{-7}$.

A.2. Production and destruction of H_3^+ and H_2D^+

The H_3^+ ions are produced at the rate $\zeta[\text{H}_2]$ by the cosmic ray ionization of H_2 followed by the reaction 10 in Table A.1. The cosmic ray ionization rate, ζ , has been estimated to be in the range $10^{-18} - 10^{-16} \text{ s}^{-1}$ (e.g. Wootten et al. 1982; Guélin et al. 1982; Duley & Williams 1984; Williams et al. 1998). The H_2D^+ ion is formed through reactions 8 (Watson 1977) and 9 (DL) of Table A.1. The former reaction is reversible in dense interstellar gas due to large abundances of both reactants on the right hand side. The forward reaction 8 is largely exothermic, which causes the equilibrium constant $K \equiv k_+/k_-$ to be strongly dependent on the kinetic temperature. In the following we need the inverse of K , $K^{-1}(T) = k_-/k_+$, for which Lee et al. (1996) have recently determined the relation $K^{-1} = 1.33 (300\text{K}/T)^{0.8} \exp(-230\text{K}/T)$ (see Table A.1).

The destruction of H_3^+ and H_2D^+ proceeds via dissociative electron recombination (reactions 6 and 7) and via reactions with neutral molecules, primarily reactions 1 and 2 with CO and the reverse of reaction 8. Reactions with such neutral species as N_2 , O, O_2 and H_2O may also have a significant contribution (e.g. Guélin et al. 1982; CWTH). The gas phase abundances of H_2O and N_2 are, however, low under dark cloud conditions (Herbst & Leung 1989; Herbst et al. 1994; Womack et al. 1992), and the reaction with O_2 is very slow (Guélin et al. 1982). Therefore, besides CO, atomic oxygen might be one of the most important destroyers of H_3^+ and H_2D^+ (CWTH).

In the following we denote the destruction rate for H_3^+ and H_2D^+ due to reactions with neutral species other than those mentioned in Table A.1 by $k[\mathcal{N}]$ and the fractional abundance of neutrals involved by $\chi(\mathcal{N})$.

The equilibrium conditions for H_3^+ and H_2D^+ are:

$$\begin{aligned} \zeta[\text{H}_2] &= \alpha_6[e^-][\text{H}_3^+] + k_1[\text{CO}][\text{H}_3^+] + \\ &+ k_+[\text{HD}][\text{H}_3^+] + \\ &+ k_9[\text{D}][\text{H}_3^+] + k[\mathcal{N}][\text{H}_3^+] \quad (\text{A12}) \\ k_+[\text{HD}][\text{H}_3^+] + k_9[\text{D}][\text{H}_3^+] &= k_-[\text{H}_2][\text{H}_2\text{D}^+] + \\ &+ \alpha_7[e^-][\text{H}_2\text{D}^+] + \\ &+ k_2[\text{CO}][\text{H}_2\text{D}^+] + \\ &+ k[\mathcal{N}][\text{H}_2\text{D}^+] . \quad (\text{A13}) \end{aligned}$$

From Eq. A12 the following formula can be obtained for the H_3^+ abundance:

$$[\text{H}_3^+] = \frac{\zeta[\text{H}_2]}{\alpha_6[e^-] + k_1[\text{CO}] + k_+[\text{HD}] + k_9[\text{D}] + k[\mathcal{N}]} . \quad (\text{A14})$$

Similarly, by arranging terms in Eq. A13 one gets for R , the $\text{H}_2\text{D}^+/\text{H}_3^+$ abundance ratio (DL Eq. 15),

$$R = \frac{k_+[\text{HD}] + k_9[\text{D}]}{k_-[\text{H}_2] + \alpha_7[e^-] + k_2[\text{CO}] + k[\mathcal{N}]} . \quad (\text{A15})$$

By using the definitions

$$\delta' \equiv k_1\chi(\text{CO}) + k_+\chi(\text{HD}) + k_9\chi(\text{D}) + k\chi(\mathcal{N}) \quad (\text{A16})$$

and

$$\delta \equiv k_- + k_2\chi(\text{CO}) + k\chi(\mathcal{N}) , \quad (\text{A17})$$

and dividing by $[\text{H}_2]$, Eqs. A14 and A15 can be written in terms of fractional abundances as follows:

$$\chi(\text{H}_3^+) = \frac{\zeta/n_{\text{H}_2}}{\alpha_6\chi(e^-) + \delta'} , \quad (\text{A18})$$

$$R = \frac{k_+\chi(\text{HD}) + k_9\chi(\text{D})}{\alpha_7\chi(e^-) + \delta} . \quad (\text{A19})$$

The quantities $n_{\text{H}_2} \delta$ and $n_{\text{H}_2} \delta'$ denote the destruction rate (s^{-1}) of H_2D^+ and H_3^+ ions, respectively, in reactions with neutral species. They differ only by the term containing the combined fractional HD and D abundances and the term k_- (which is negligible at low temperatures i.e. below 20 K):

$$\delta' - \delta = k_+\chi(\text{HD}) + k_9\chi(\text{D}) - k_- . \quad (\text{A20})$$

Note that when one assumes that $[\text{D}] = 0$ and that $R \approx 3r$ (see Eq. A8), then Eq. A19 becomes equivalent to Eq. (1) of CWTH. Eq. (2) of CWTH can be derived by solving the ratio $\chi(\text{HCO}^+)/\chi(\text{CO})$ from Eq. A10, and substituting $\chi(\text{H}_3^+)$ from Eq. A18. Assuming that the term containing R and r on the right hand side of Eq. A10 is of order 1, one obtains the formula:

$$\frac{\chi(\text{HCO}^+)}{\chi(\text{CO})} = \frac{k_1\zeta/n_{\text{H}_2}}{\alpha_4\chi(e^-)(\alpha_6\chi(e^-) + \delta')} . \quad (\text{A21})$$

The abundance of HD is far greater than that of other deuterated molecules (see below). However, according to the model of DL the relative abundance of atomic deuterium may be of significance. Therefore, it seems advisable to assume that practically all deuterium is in the form of HD and free D atoms. The atomic D/H ratio in the solar neighbourhood is $1.65 \cdot 10^{-5}$ (Linsky et al. 1995) indicating that the combined abundance of HD and D is very small compared with molecular hydrogen. If it is assumed that all hydrogen is in molecular form then the combined HD and D abundance is given by:

$$\chi(\text{HD}) + \chi(\text{D}) \approx 2 \frac{[\text{D}]}{[\text{H}]_{\text{local ISM}}} = 3.3 \cdot 10^{-5} . \quad (\text{A22})$$

A.3. Production and destruction of D

Atomic deuterium is produced in reaction 5, and in the dissociative recombination of H_2D^+ (reaction 7, Larsson et al. 1996). The contribution of this reaction to the production of D was neglected in DL due to the fact that Smith & Adams (1984)

determined a very low *upper limit* of $2 \cdot 10^{-8} \text{ cm}^3 \text{ s}^{-1}$ for the dissociative recombination rate of H₃⁺, and thus also for H₂D⁺. Larsson et al. (1996) determined for $\alpha_7 = \alpha(\text{H}_2\text{D}^+)$ a value of $6 \cdot 10^{-8} \text{ cm}^3 \text{ s}^{-1}$ at 300 K, which is about one half of the corresponding recombination rate for H₃⁺ at the same temperature (Sundström et al. 1994). For $\alpha(\text{H}_3^+)$ the temperature dependence of $\alpha(\text{H}_3^+) = 4.6 \cdot 10^{-6} T^{-0.65} \text{ cm}^3 \text{ s}^{-1}$ (Sundström et al. 1994). Assuming a similar power law for α_7 , its value at 95 K is $1.3 \cdot 10^{-7} \text{ cm}^3 \text{ s}^{-1}$, i.e. one half of $\alpha(\text{DCO}^+) = \alpha_5$.

According to DL atomic deuterium is destroyed by reactions 3 and 9 and in collisions with dust grains at rate $2k_g[\text{H}_2]$. DL suggest that $k_9 \approx 1.7 \cdot 10^{-9} \text{ cm}^3 \text{ s}^{-1}$. Estimates for k_g range from $5 \cdot 10^{-18}$ to $5 \cdot 10^{-17} \text{ cm}^3 \text{ s}^{-1}$, the most commonly used value being $3 \cdot 10^{-17} \text{ cm}^3 \text{ s}^{-1}$ (Duley & Williams 1984). In their OD study, Croswell & Dalgarno (1985) adopt a slightly lower value of $k_g = 1.5 \cdot 10^{-17} \text{ cm}^3 \text{ s}^{-1}$.

In equilibrium, the abundance of D is given by

$$[\text{D}] = \frac{\alpha_5[e^-][\text{DCO}^+] + \frac{4}{5}\alpha_7[e^-][\text{H}_2\text{D}^+]}{2k_g[\text{H}_2] + k_3[\text{HCO}^+] + k_9[\text{H}_3^+]}. \quad (\text{A23})$$

The factor $\frac{4}{5}$ in front of α_7 comes from the branching ratios of reaction 7 as determined by Larsson et al. (1996). Eq. A23 differs from the corresponding expression in DL (their Eq. 12) by the latter term in the numerator.

DL derive estimates for the fractional electron abundance as a function of r by substituting the counterpart of Eq. A23 into that of Eq. A6. With the modifications introduced here this procedure becomes a little bit more laborious. By defining the quantities β and γ by

$$\beta \equiv \frac{2k_g + k_9\chi(\text{H}_3^+)}{k_3\chi(\text{HCO}^+)} \quad \text{and} \\ \gamma \equiv \frac{2k_g + k_3\chi(\text{HCO}^+)}{k_9\chi(\text{H}_3^+)}, \quad (\text{A24})$$

Eq. A23 can be rewritten as

$$\frac{\chi(\text{D})}{\chi(e^-)} = \frac{\alpha_5}{k_3} \frac{r}{1+\beta} + \frac{4}{5} \frac{\alpha_7}{k_9} \frac{R}{1+\gamma}. \quad (\text{A25})$$

Combining Eqs. A5 and A10, the following expression for ξ is obtained:

$$\xi = \frac{k_3}{\alpha_4} \frac{\chi(\text{D})}{\chi(e^-)} \frac{1+R}{1+r} = \left\{ \frac{r}{1+\beta} + \frac{4\alpha_7}{5\alpha_4} \frac{R}{1+\gamma} \right\} \frac{1+R}{1+r}. \quad (\text{A26})$$

In this expression we have made use of the rate constant equalities in Lee et al. (1996): $k_2 = k_1$, $k_9 = k_3$, and $\alpha_5 = \alpha_4$. Substitution of Eq. A26 into Eq. A6 leads to a quadratic equation for R :

$$aR^2 + bR - c = 0, \quad (\text{A27})$$

where

$$a = \frac{4\alpha_7}{5\alpha_4} \frac{1}{1+\gamma}, \\ b = \frac{1}{3} + \frac{1}{3} \frac{1-2\beta}{1+\beta} r + \frac{4\alpha_7}{5\alpha_4} \frac{1}{1+\gamma} \quad \text{and} \\ c = \frac{\beta}{1+\beta} r. \quad (\text{A28})$$

Eq. A27 can be solved by assuming certain values for the H₃⁺ abundance and the rate constant k_g . The solution can then be used in Eq. A10 to obtain an estimate for the fractional electron abundance $\chi(e^-)$. This can be further substituted into Eq. A19 to derive an estimate for $\chi(\mathcal{N})$, and finally, an estimate of the quantity ζ/n_{H_2} can be derived from Eq. A14.

The derived values of $\chi(e^-)$ and ζ/n_{H_2} depend directly on the assumed ratio $\chi(\text{H}_3^+)/\chi(\text{HCO}^+)$, whereas estimates for R are sensitive to the rate constant k_g . For larger values of k_g , i.e. $10^{-17} - 10^{-16} \text{ cm}^3 \text{ s}^{-1}$, R lies close to its upper limit $\sim 3r$, but remains well below it near the lower boundary of the probable range ($\sim 10^{-18} \text{ cm}^3 \text{ s}^{-1}$).

If the reaction rate constants and the combined abundance of HD and D are assumed to be known, the model described here contains five unknowns (R , $\chi(e^-)$, $\chi(\text{D})$, $\chi(\text{H}_3^+)$ and ζ/n_{H_2}) and five independent equations: (A10), (A18), (A19), (A25) and (A27). Bearing in mind that the derived set of equations probably does not fully describe the true situation (e.g. metal abundances and interaction with grains are omitted) no attempt at their proper solution has been made. Instead, we have used results from previous studies to obtain reasonable initial values of some parameters and solved the set of equations in an iterative manner as described in the text.

Appendix B: estimation of temperatures with the rotation diagram method

The rotational diagram method for a symmetric top molecule is based on comparison of the intensities of the spectral line components arising from rotational levels with different energies but lying close to each other in frequency. More detailed description of the method can be found e.g. in Churchwell & Hollis (1983) and Bergin et al. (1994).

Assuming optically thin emission, the integrated brightness temperature of a spectral line component as a function of the column density of the molecules in the upper transition level, N_u , is:

$$\int T_B(v) dv = \frac{1}{\eta} \int T_A^*(v) dv \\ = \frac{2\pi^2}{3} \frac{\nu\mu^2}{k\varepsilon_0} \frac{S_{J,K}}{2J+1} \left\{ 1 - \frac{F(T_{\text{bg}})}{F(T_{\text{ex}})} \right\} N_u, \quad (\text{B1})$$

where η is the beam–source coupling efficiency, ν is the line rest frequency, μ is the permanent dipole moment of the molecule, k is the Boltzmann constant, ε_0 is the vacuum permittivity, T_{bg} is the (cosmic) background radiation temperature and T_{ex} is the excitation temperature of the transition being observed. The quantity $S_{J,K}$ is the so called line strength of the transition $(J, K) \rightarrow (J-1, K)$ defined as

$$S_{J,K} \equiv \frac{J^2 - K^2}{J}. \quad (\text{B2})$$

The function $F(T)$ is defined by

$$F(T) \equiv \frac{1}{e^{h\nu/kT} - 1}, \quad (\text{B3})$$

where h is the Planck constant. Note that the integration is performed with respect to the radial velocity v .

Assuming rotational equilibrium at a temperature T_{rot} , the column density N_u can be obtained from the total column density of the molecule N according to:

$$N_u = g_J g_K g_I \frac{e^{-E_u/kT_{\text{rot}}}}{Z} N, \quad (\text{B4})$$

where g_J and g_K are the statistical weights due to angular momentum and its projection onto a given axis, respectively ($g_J = 2J + 1$; $g_K = 1$ when $K = 0$, and $g_K = 2$ when $K \neq 0$). The statistical weight g_I takes account of the spins of the three hydrogen nuclei (each having $I = \frac{1}{2}$) and takes the value 4 when $K = 0, 3, 6, \dots$ and 2 when $K = 1, 2, 4, 5, \dots$ (see Ch. 3 and Table 3-6 in Townes & Schawlow 1975). The partition function, Z , is given by

$$Z = \sum_{J=0}^{\infty} \sum_{K=0}^J g_J g_K g_I e^{-E(J,K)/kT_{\text{rot}}}. \quad (\text{B5})$$

By combining Eqs. B1 and B4, and assuming that $F(T_{\text{bg}}) \ll F(T_{\text{ex}})$ one obtains

$$\ln\left\{\frac{\int T_A^* dv}{\eta \nu S_{J,K} g_I g_K}\right\} = \ln\left\{\frac{2\pi^2 \mu^2 N}{3k \varepsilon_0 Z}\right\} - \frac{1}{T_{\text{rot}}} \frac{E_u}{k}. \quad (\text{B6})$$

The unknowns in Eq. B6 are the total column density N and the rotational temperature T_{rot} , both of which can be determined by observing several transitions belonging to different K -ladders: In LTE T_{rot} is constant and the observed values of the left hand side should lie on straight line when plotted as a function of E_u/k . The slope of this line is determined by the reciprocal of T_{rot} , and its intersection with the $E_u/k = 0$ axis gives the ratio N/Z .

References

- Anderson I.M., Harju J., Knee L.B.G., Haikala L.K., 1997a, A&A 321, 575 (A97a)
- Anderson I.M., Harju J., Haikala L.K., 1997b, A&A 326, 366 (A97b)
- Bally J., Langer W.D., 1982, ApJ 255, 143
- Bergin E.A., Goldsmith P.F., Snell R.L., Ungerechts H., 1994, ApJ 431, 674
- Bergin E.A., Plume R., Williams J.P., Myers P.C., 1999, ApJ 512, 724
- Bertsch D.L., Dame T.M., Fichtel C.E., 1993, ApJ 416, 587
- Booth R.S., Delgado G., Hagström M., et al., 1989, A&A 216, 315
- Brown P.D., Millar T.J., 1989, MNRAS 237, 661
- Brown R.D., Rice E.H.N., 1986, MNRAS 223, 429
- Caselli P., Walmsley C.M., Terzieva R., Herbst E., 1998, ApJ 499, 234 (CWTH)
- Ceccarelli C., Castets A., Loinard L., Caux E., Tielens A.G.G.M., 1998, A&A 338, L43
- Charnley S.B., 1997, MNRAS 291, 455
- Charnley S.B., Roberge W.G., 1992, In: Singh P.D. (ed.) *Astrochemistry of Cosmic Phenomena*. IAU Symposium No. 150, Kulwer Academic Publishers, Dordrecht, p. 155
- Chin N.-Y., Henkel C., Millar T.J., Whiteoak J.B., Mauersberger R., 1996, A&A 312, L33
- Churchwell E., Hollis J.M., 1983, ApJ 272, 591
- Croswell K., Dalgarno A., 1985, ApJ 289, 618
- Dalgarno A., Lepp S., 1984, ApJ 287, L47
- Duley W.W., Williams D.A., 1984, *Interstellar Chemistry*. Academic Press Inc. (London) LTD
- Graham J.A., 1991, In: Reipurth B. (ed.) *Low Mass Star Formation in Southern Molecular Clouds*. ESO Scientific Report No. 11, Garching bei München, p. 185
- Guélin M., Langer W.D., Snell R.L., Wootten H.A., 1977, ApJ 217, L165
- Guélin M., Langer W.D., Wilson R.W., 1982, A&A 107, 107
- Harju J., Haikala L.K., Mattila K., et al., 1993, A&A 278, 569 (H93)
- Harjunpää P., Mattila K., 1996, A&A 305, 920
- d'Hendecourt L.B., Allamandola L.J., Baas F., Greenberg J.M. 1982, A&A 109, L12
- d'Hendecourt L.B., Allamandola L.J., Greenberg J.M., 1985, A&A 152, 130
- Herbst E., 1982, A&A 111, 76
- Herbst E., Leung, 1989,
- Herbst E., Lee, Howe, Millar, 1994,
- Juvela M., 1997, A&A 322, 943
- Kramer C., Alvé J., Lada C., et al., 1999, A&A 342, 257
- Larsson M., Lepp S., Dalgarno A., et al., 1996, A&A 309, L1
- Lee H.-H., Bettens R.P.A., Herbst E., 1996, A&AS 119, 111
- Linsky J.L., Diplas A., Wood B.E., et al., 1995, ApJ 451, 335
- Loren R.B., Wootten A., Wilking B.A., 1990, ApJ 365, 269
- Monteiro T.S., 1985, MNRAS 214, 419
- Press W.H., Flannery B.P., Teukolsky S.A., Vetterling W.T., 1986, *Numerical Recipes*. Cambridge University Press, p. 502
- Shalabiea O.M., Greenberg J.M., 1994, A&A 290, 266
- Smith D., Adams N.G., 1984, ApJ 284, L13
- Smith D., Spanel P., Millar T.J., 1994, MNRAS 266, 31
- Strong A.W., 1987, In: Morfill G.E., Scholer M. (eds.) *Physical Processes in Interstellar Clouds*. NATO ASI Series, D. Reidel Publishing Company, Dordrecht, p. 75
- Sundström G., Mowat J.R., Danared H., et al., 1994, Sci 263, 785
- Tielens A.G.G.M., Allamandola L.J., 1987, In: Hollenbach D.J., Thronson Jr. H.A. (eds.) *Interstellar Processes*. D. Reidel Publishing Company, Dordrecht, p. 397
- Townes C.H., Schawlow A.L., 1975, *Microwave Spectroscopy*. Dover Publications Inc., New York
- Watson W.D., 1977, In: Audouze J. (ed.) *CNO, Isotopes in Astrophysics*. Reidel Publishing Company, Dordrecht, p. 105
- Watson W.D., Snyder L.E., Hollis J.M., 1978, ApJ 222, L145
- Wilking B.A., Harvey P.M., Joy M., Hyland A.R., Jones T.J., 1985, ApJ 293, 165
- Wilking B.A., McCaughrean, Burton M.G., et al., 1997, AJ 114, 2029
- Williams J.P., Bergin E.A., Caselli P., Myers P.C., Plume R., 1998, ApJ 503, 689
- Wilson T.L., Rood R.T., 1994, ARA&A 32, 191
- Womack M., Ziurys L.M., Wyckoff S., 1992, ApJ 393, 188
- Wootten A., Shah R., 1998, A&AS 193, 7206
- Wootten A., Loren R.B., Snell R.L., 1982, ApJ 255, 160
- Wootten A., Snell R.L., Glassgold A.E., 1979, ApJ 234, 876
- Xie T., Allen M., Langer W.D., 1995, ApJ 440, 674